Earth-Science Reviews 177 (2018) 458–477

Contents lists available at ScienceDirect

Earth-Science Reviews

journal homepage: www.elsevier.com/locate/earscirev

A new assessment of modern climate change, China—An approach based on paleo-climate

Yu Li*, Yuan Liu, Wangting Ye, Lingmei Xu, Gengrui Zhu, Xinzhong Zhang, Chengqi Zhang

Key Laboratory of Western China's Environmental Systems, Ministry of Education, College of Earth and Environmental Sciences, Center for Hydrologic Cycle and Water Resources in Arid Region, Lanzhou University, Lanzhou 730000, China

ARTICLE INFO

Keywords:
Assessment
Holocene
Climate change
China
Paleo-climate
Asian monsoon

ABSTRACT

China is the country with the most population in the world, and its climate is extremely diverse due to tremendous differences in latitude, longitude, and altitude, ranging from tropical in the far south to subarctic in the far north and alpine in the higher elevations of the Qinghai-Tibetan Plateau. Accurate assessment of its modern climate change is conductive to addressing global warming threat. Along with the development of Past Global Changes (PAGES) research, the focus has changed from paleo-climate reconstructions to using paleo-data for assessing the present and predicting the future. Previous studies have been devoted to climate change assessment using modern climate observations and simulations. This paper presents a new assessment approach based on the mid-Holocene, which provides a naturally oriented warming that can be compared to modern human-made global warming. A variety of climatic data, including modern observations, paleo-climate records, CMIP5 (Coupled Model Intercomparison Project Phase 5) and PMIP3 (Paleoclimate Modelling Intercomparison Project 3) simulations, as well as lake level models, were applied in this synthesis. Numerical climate classification was introduced to evaluate climate change impacts to Chinese climate zones on various time scales. The results show that winter and summer seasons have different response to the naturally oriented mid-Holocene warming but human-made global warming makes the warming trend appear in all seasons. Temperate and continental dry winter climates expand dramatically during the mid-Holocene warm period; however, the future global warming could have few impacts to Chinese climate zones. Furthermore, the East Asian summer monsoon was strengthened obviously by the mid-Holocene warm climate and strong low-latitude insolation. There is no consistent trend both for the winter and summer monsoon on the background of human-made global warming. In this study, a new benchmark was established based on paleo-climate to evaluate the impacts of human-made global warming.

1. Introduction

Modern climate change is a major global issue of common concern to the international community. A great number of observations in recent 100 years show that the earth's climate is now experiencing significant change characterized by global warming (Hansen et al., 2010; Jones and Wigley, 2010). The Fifth Assessment Report of the Intergovernmental Panel on Climate Change (IPCC) has clearly indicated that most of the global warming observed over the past 50 years was unequivocally induced by the increase in concentrations of greenhouse gases (Working Group I for the Fifth Assessment Report of the Intergovernmental Panel on Climate Change, 2013). An accurate and comprehensive assessment to modern human-made climate change lays the foundation for addressing modern climate issues. China covers a wide range of latitudes and longitudes, and both its topography and climate are diverse and complex. Tropical, subtropical, warm and cold temperate, continental, as well as highland climates appear in different regions. Furthermore, monsoon climate, caused by different general circulation patterns between winter and summer seasons and differences in the heat-absorbing capacity of the continent and the ocean, strongly affects the overall pattern of Chinese climate (Webster et al., 1998; Wang and Lin, 2002).

The trend of climate change in China is generally consistent with that of global climate change, experiencing warming climate in the

* Corresponding author.
E-mail address: liyu@lzu.edu.cn (Y. Li).

https://doi.org/10.1016/j.earscirev.2017.12.017
Received 23 January 2017; Received in revised form 5 December 2017; Accepted 19 December 2017
Available online 24 December 2017
0012-8252/ © 2017 Elsevier B.V. All rights reserved.

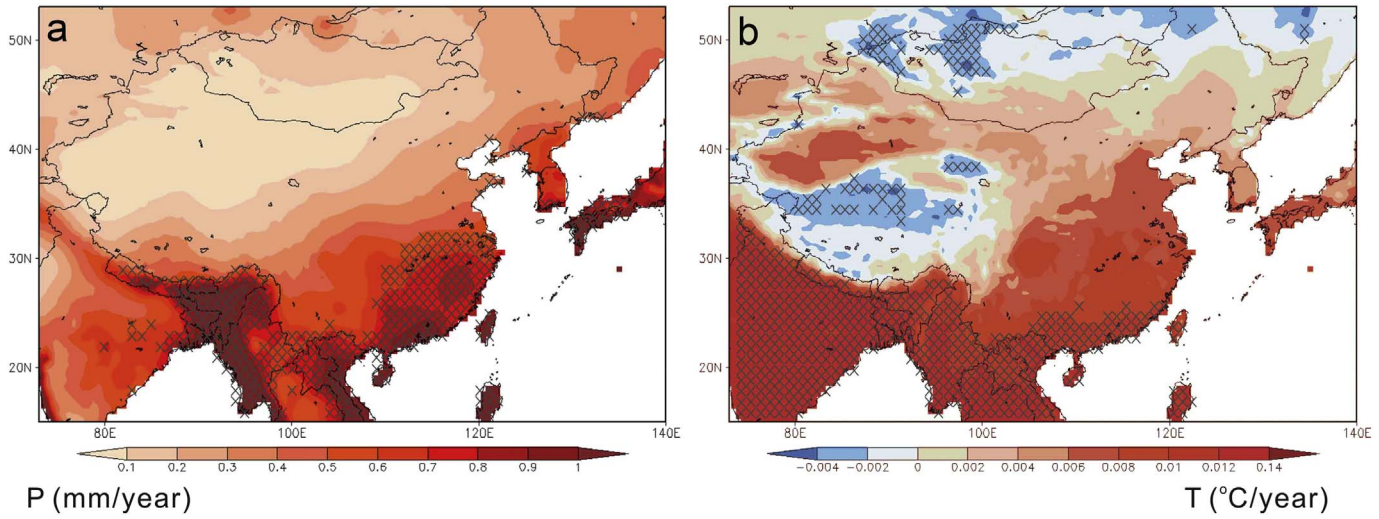

Fig. 1. Linear trends of precipitation and temperature in China from 1960 to 2013.

Table 1
Description of Köppen climate symbols and defining criteria.

1st	2st	Description	Criteria[a]
A		Tropical	$T_{cold} \geq 18$ °C
	f	-Rainforest	$P_{dry} \geq 60$ mm
	m	-Monsoon	$P_{dry} \leq 60$ mm & $P_{dry} \geq$ (100–MAP/25)mm
	w	-Savannah	$P_{dry} \leq 60$ mm & $P_{dry} <$ (100–MAP/25)mm
B		Arid	MAP $< 10\ P_{threshold}$
	s	-Steppe	MAP $\geq 5\ P_{threshold}$
	w	-Desert	MAP $< 5\ P_{threshold}$
C		Temperate	$T_{hot} > 10$ °C & 0 °C $< T_{cold} < 18$ °C
	s	-Dry Summer	$P_{sdry} < 40$ mm & $P_{sdry} < P_{wwet}/3$
	w	-Dry Winter	$P_{wdry} < P_{swet}/10$
	f	-Without dry season	Not(Cs)or(Cw)
D		Continental	$T_{hot} > 10$ °C & $T_{cold} \leq 0$ °C
	w	-Dry Winter	$P_{wdry} < P_{swet}/10$
	f	-Without dry season	$P_{wdry} \geq P_{swet}/10$
E		Polar	$T_{hot} < 10$ °C
	T	-Tundra	$T_{hot} \geq 0$ °C
	F	-Frost	$T_{hot} < 0$ °C

[a] MAP = mean annual precipitation, MAT = mean annual temperature, Thot = temperature of the hottest month, Tcold = temperature of the coldest month, Pdry = precipitation of the driest month, Psdry = precipitation of the driest 1 month in summer, Pwdry = precipitation of the driest month in winter, Pswet = precipitation of the wettest month in summer, Pwwet = precipitation of the wettest month in winter, Pthreshold = varies according to the following rules (if 70% of MAP occurs in winter then Pthreshold = 2 × MAT, if 70% of MAP occurs in summer then Pthreshold = 2 × MAT + 28, otherwise Pthreshold = 2 × MAT + 14).

20th century, and its mean surface temperature has a similar increasing trend with the global one (Wang and Gong, 2000). For the second half of the 20th century, annual precipitation has no significant trends and the spatial distribution of precipitation trends across China is uneven (Zhai et al., 1999). Decreasing trends in the number of rainy days and the longest durations of consecutive rainfall have been detected (Zhai et al., 2005). China has suffered from frequent extreme weather conditions, such as extremely high temperatures, frequent storms and floods, severe droughts and landslides in recent decades (You et al., 2011). In 2015, China's Ministry of Science and Technology officially released China's "Third National Assessment Report on Climate Change" (The Editorial Board of Third National Assessment of Report on Climate Change of China, 2015). The findings of the report revealed that average temperatures across China have risen by 0.9 to 1.5 °C from 1909 to 2011. This trend will further intensify in the future and temperatures across most of China will rise another 1.3 to 5.0 °C by the end of this century compared to the global average of 1.0 to 3.7 °C. Under the threat of global warming, it is an urgent need to assess modern climate change in China comprehensively. Previous studies mostly focused on assessment using modern observations and simulations to evaluate and predict global warming impacts. However, it lacks a comparison of processes and mechanisms between naturally oriented and human-made warming, which makes us more aware of human impacts on climate change.

The PAGES (Past Global Changes) project is an international effort to coordinate and promote past global change research, and supports research which aims to understand the Earth's past environment in order to obtain better predictions of future climate and environment, and inform strategies for sustainability (PAGES Scientific Steering Committee, 2009). As a core project of Future Earth, its main task has changed from paleo-climate reconstructions to using paleo-data for climate assessment and prediction. The middle Holocene or a period roughly from 7000 to 5000 years ago, was warmer than the present, and terms like the Hypsi-thermal or Climatic Optimum have all been used to refer to this warm period that marked the middle of the current interglacial period (Kerwin et al., 1999; Marcott et al., 2013). The naturally oriented astronomical climate forcing mechanism is responsible for the mid-Holocene warming in the northern hemisphere, which provides us an ideal analog for modern global warming but with different mechanisms. Shi et al. (1993) firstly proposed the mid-Holocene Climatic Optimum in China according to proxy data of various sedimentary sequences and pointed out that the mid-Holocene annual mean temperature was roughly higher than modern times, about 1 °C in South China, 2 °C in the Yangtze Valley, 3 °C in North China and Northeast China. This view was widely accepted by subsequent studies (Li et al., 1995; Tang et al., 1998; Xiao et al., 2006; Herzschuh et al., 2010). However, compared with the mid-Holocene ubiquitous warming trend in China, the mid-Holocene precipitation pattern that is strongly influenced by the Asian summer monsoon is complex and drawn much attention from paleo-climatologists (An et al., 2000; He et al., 2004; Herzschuh, 2006; Chen et al., 2008; Y. Wang et al., 2010; T. Wang

Table 2
Holocene paleo-climatic records including lake levels and paleo-temperature in China.

ID	Site	Lat.	long.	Alt. (m)	Lake-level	Temperature	References
					6 ka-PI	6 ka-PI	
1	Hulun Lake	49°0′N	117°25′E	545	High	\	Wang and Ji, 1995
2	Xingkai Lake	44°57′N	132°25′E	69	High	\	Wu and Shen, 2010a, 2010b
3	Erlongwan Maar Lake	42°18′N	126°22′E	722	High	\	Y.Y. Liu et al., 2008b; You et al., 2011
4	Daihai Lake	40°33′N	112°39′E	1220	High	\	Xiao et al., 2004; Xu et al., 2010
5	Dajiu Lake	31°28′ N	110°04′E	1780	Low	\	Ma et al., 2008; Zhu et al., 2006
6	Poyang Lake	29°01′N	116°08′E	1324	Low	\	Ma et al., 2004; Jiang and Piperno, 1999
7	Dahu Lake	24°41′N	115°00′E	255	High	\	Zhong et al., 2010; Xiao et al., 2007
8	Huguangyan Maar Lake	21°09′N	110°17′E	87.6	High	\	Liu et al., 2005; Mingram et al., 2004
9	Xingyun Lake	24°20′N	102°47′E	1740	High	\	Zhang et al., 2014; Hodell et al., 1999
10	Erhai Lake	25°47′N	100°12′E	1974	High	\	Shen et al., 2005b, 2006
11	Lugu Lake	27°42′N	100°50′E	2690	High	\	Zheng et al., 2014
12	Naleng Lake	31°06′N	99°45′E	4200	High	\	Kramer et al., 2010a, 2010b
13	Zhuye Lake	39°03′N	103°40′E	1309	High/similar	\	Q. Li et al., 2009b
14	Qinghai Lake	36°32′N	99°36′E	3200	Similar	\	Shen et al., 2004, 2005a
15	Gahai Lake	37°08′N	97°33′E	2850	Low	\	Chen, 2010
16	Chen Co	28°56′N	90°35′E	4420	High	\	Zhu et al., 2009;
17	Nam Co	30°42′N	90°40′E	4718	High	\	Li et al., 2011; Zhu et al., 2008
18	Zigetang Co	32°04′N	90°50′E	4560	Low	\	S.J. Li et al., 2009
19	Bangong Co	33°40′N	79°30′E	4241	High	\	Van Campo et al., 1996; Fan et al., 1996
20	Bosten Lake	42°05′N	87°03′E	1048	High	\	Zhang et al., 2007; Zhang et al., 2010
21	Balikun Lake	43°40′N	92°48′E	1575	High	\	Xue and Zhong, 2011; Tao et al., 2010
22	Wulungu Lake	47°12′N	87°17′E	479	High	\	Jiang et al., 2007; X. Liu et al., 2008
23	Otindag sandy land	42°50′N	115°16′E	1240	\	High	Li et al., 1995
24	Daihai Lake	40°33′N	112°39′E	1220	\	High	Xiao et al., 2006
25	Luanhaizi Lake	37°59′N	101°35′E	3200	\	High	Herzschuh et al., 2010
26	Koucha Lake	34°0′N	97°12′E	4540	\	High	Herzschuh et al., 2009
27	Ren Co	30°43′N	96°41′E	4450	\	High	Tang et al., 1998
28	Guliya ice core	35°17′N	81°29′E	6710	\	High	He et al., 2003

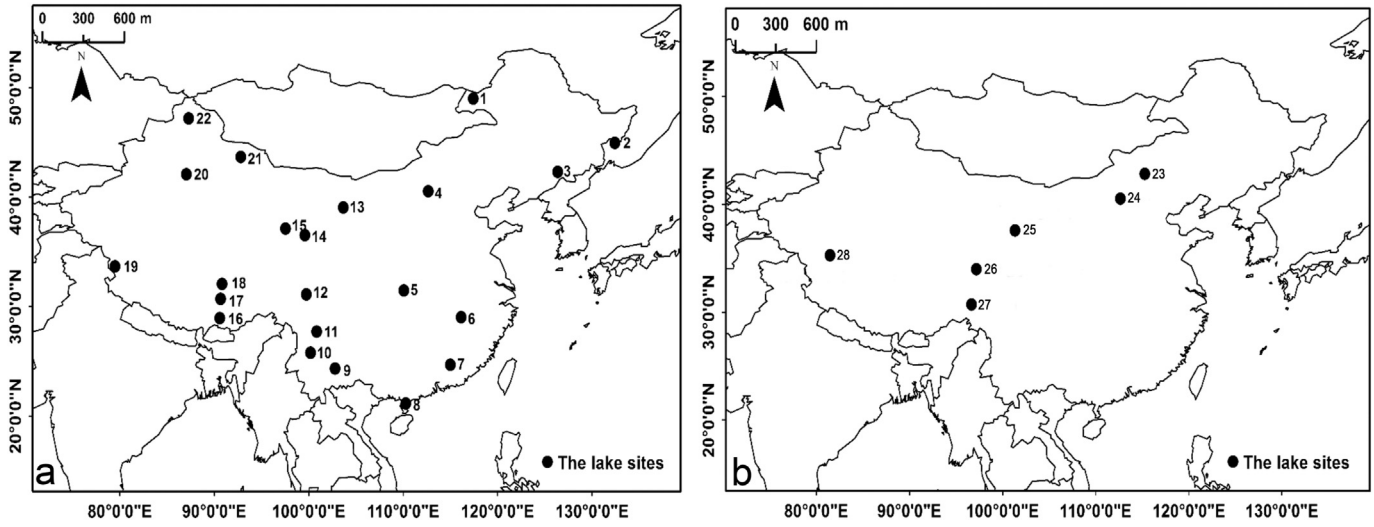

Fig. 2. Spatial distribution of the paleo-lake records (left) and paleo-temperature reconstructions (right).

Table 3
Description of PMIP3 models used in this study.

Model ID	Country	Number of grids (lon)	Number of grids (lat)	Levels	Resolution (lon °)	Resolution (lat °)
CCSM4	USA	288	192	17	1.25	0.9375
CNRM-CM5	France	256	128	17	1.40625	1.40625
CSIRO	Australia	192	96	18	1.875	1.875
EC-EARTH	European	320	160	17	1.125	1.125
FGOALS	China	128	108	17	2.8125	1.666667
GISS-E2	USA	144	89	17	2.5	2.022472
MPI-ESM-P	Germany	192	96	25	1.875	1.875
MRI-CGCM3	Japan	320	160	23	1.125	1.125
bcc-csm1-1	China	128	64	17	2.8125	2.8125
IPSL-CM5A-LR	France	96	96	17	3.75	1.875

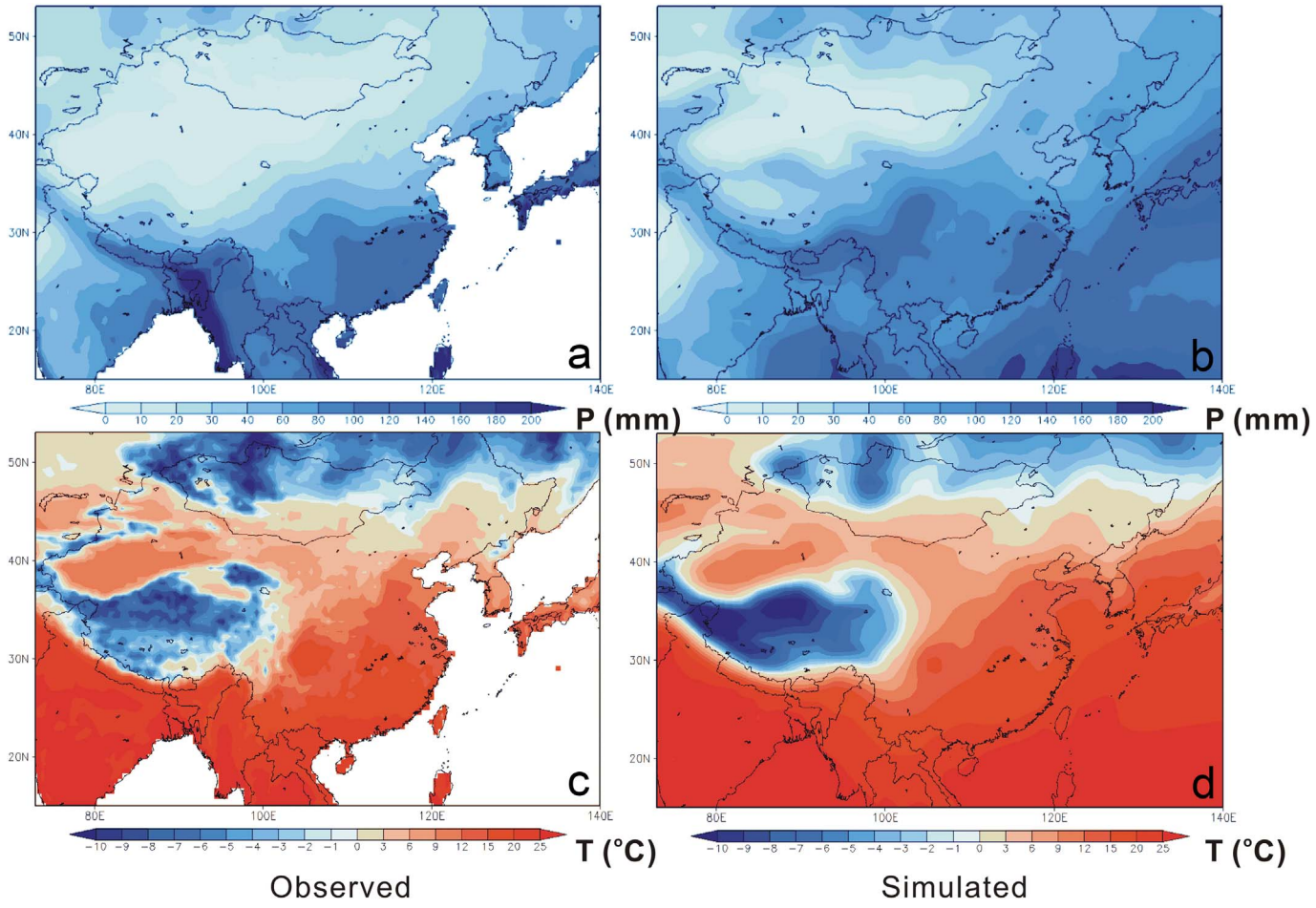

Fig. 3. A comparison between observed and simulated (PMIP3 models) monthly mean precipitation and annual mean temperature at 0 ka.

Table 4
Description of CMIP5 models used in this study.

Model ID	Country	Number of grids (lon)	Number of grids (lat)	Levels	Resolution (lon °)	Resolution (lat °)
CMCC CESM	Italy	96	48	33	3.75	3.75
CNRM-CM5	France	256	128	17	1.40625	1.40625
FGOALS	China	128	108	17	2.8125	1.666667
GISS-E2	USA	144	89	17	2.5	2.022472
HadGEM2	South Korea	192	144	17	1.875	1.25
Inmcm4	Russia	180	120	17	2	1.5
MPI-ESM-LR	Germany	192	96	25	1.875	1.875
MRI-CGCM3	Japan	320	160	23	1.125	1.125

et al., 2010; Li et al., 2014). An et al. (2000) initially suggested that Holocene precipitation changes were synchronous in China. Herzschuh (2006) reviewed 75 records from East Asia and found that the Holocene precipitation patterns differed between Central Asia and some parts of the Asian monsoon domain. Chen et al. (2008) analyzed the absolutely dated Holocene precipitation records for the Asian monsoon domain and arid Central Asia and concluded that Holocene millennium-scale climate patterns differ for the two regions. Y. Wang et al. (2010) and T. Wang et al. (2010) synthesized 92 proxy records of moisture/precipitation change in East and arid China that reveal a strong spatial heterogeneity during the Holocene. The different precipitation pattern is mainly due to various responses to millennial-scale changes in the Asian monsoon and the westerlies (Li et al., 2014).

In this study, we chose the mid-Holocene as a naturally oriented warm period to analyze the process and mechanism difference between modern human-made warming and natural warming. Data and methods include modern observations, numerical climate classification, paleo-climate records in China, paleo-lake level models, CMIP5 (Coupled Model Intercomparison Project Phase 5) and PMIP3 (Paleoclimate Modelling Intercomparison Project 3) simulations and difference analysis of 500 hpa geopotential height fields and 850 hpa wind fields on various time scales. This research will contribute to our understanding regarding human

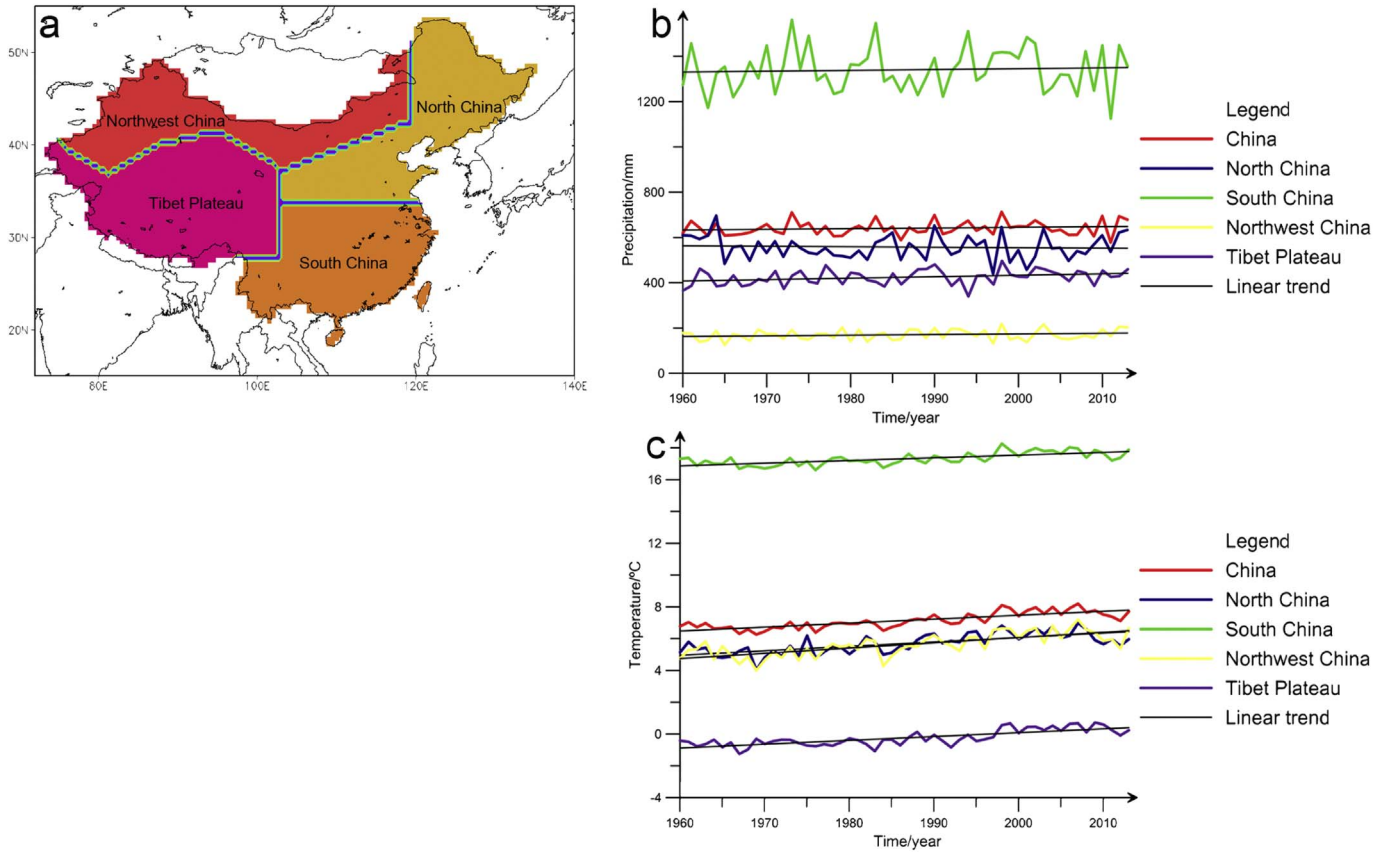

Fig. 4. Variations of regional mean precipitation and temperature in China from 1960 to 2013.

impacts to natural climate change.

2. Data, simulations and methods

2.1. Modern observation data

The modern observation data in China are based on a Climatic Research Unit (CRU) updated gridded climate dataset (referred to as CRU TS3.22) from monthly observations at meteorological stations across the world's land areas (Harris et al., 2013). Climatic Research Unit (CRU) monthly climate archives come through the auspices of the World Meteorological Organization (WMO) in collaboration with the US National Oceanographic and Atmospheric Administration (NOAA, via its National Climatic Data Center, NCDC). Station anomalies were interpolated into 0.5° latitude/longitude grid cells covering the global land surface, and combined with an existing climatology to obtain absolute monthly values. The dataset includes mean temperature, diurnal temperature range, precipitation, wet-day frequency, vapor pressure, and cloud cover, six mostly independent climate variables. CRU TS3.22 includes diagnostics associated with each interpolated value that indicate the number of stations used in the interpolation, allowing determination of the reliability of values in an objective way. Choosing this global modern observation dataset is to match CMIP5 (Coupled Model Intercomparison Project Phase 5) and PMIP3 (Paleoclimate Modelling Intercomparison Project 3) models used in this research, all of which are on a global scale. Fig. 1 shows the linear change trends of precipitation and temperature from 1960 to 2013 according to this dataset. Chinese monthly surface temperature and precipitation gridded dataset (0.5° × 0.5°) from National Meteorological Information Center, China Meteorological Administration is also used in this study to verify the global dataset (http://cdc.cma.gov.cn).

2.2. Climate classification

Köppen-Geiger climate classification is one of the most widely used numerical climate classification system, which is developed according to annual monthly cycles of precipitation and temperature that are connected to vegetation distribution (Peel et al., 2007). The Köppen-Geiger climate classification used in this research identifies five main climate regions: tropical (A), arid (B), temperate (C), continental (D), and polar (E) (Table 1). The A-, C-, and D-zones are further subdivided closely related the seasonality of temperature and precipitation (Baker et al., 2010).

Based on a series of 0.5° × 0.5° monthly gridded precipitation and temperature datasets during 1961–2013 (see Section 2.1), and a 0.5° × 0.5° gridded elevation data downloaded from http: //www.ngdc.noaa.gov/mgg/topo/globe.html, we divided China's climate into 5 main climate groups, 12 types and 28 subtypes according to criteria of Table 1. Chinese main climate groups are Arid (B), Temperate (C), Continental (D) and Polar (E), and main climate types include Steppe climate (Semi-arid) (Bs), Desert climate (Bw), Mild temperate with dry winter (Cw), Fully humid (Cf), Snow with dry winter (Dw), Tundra climate (ET).

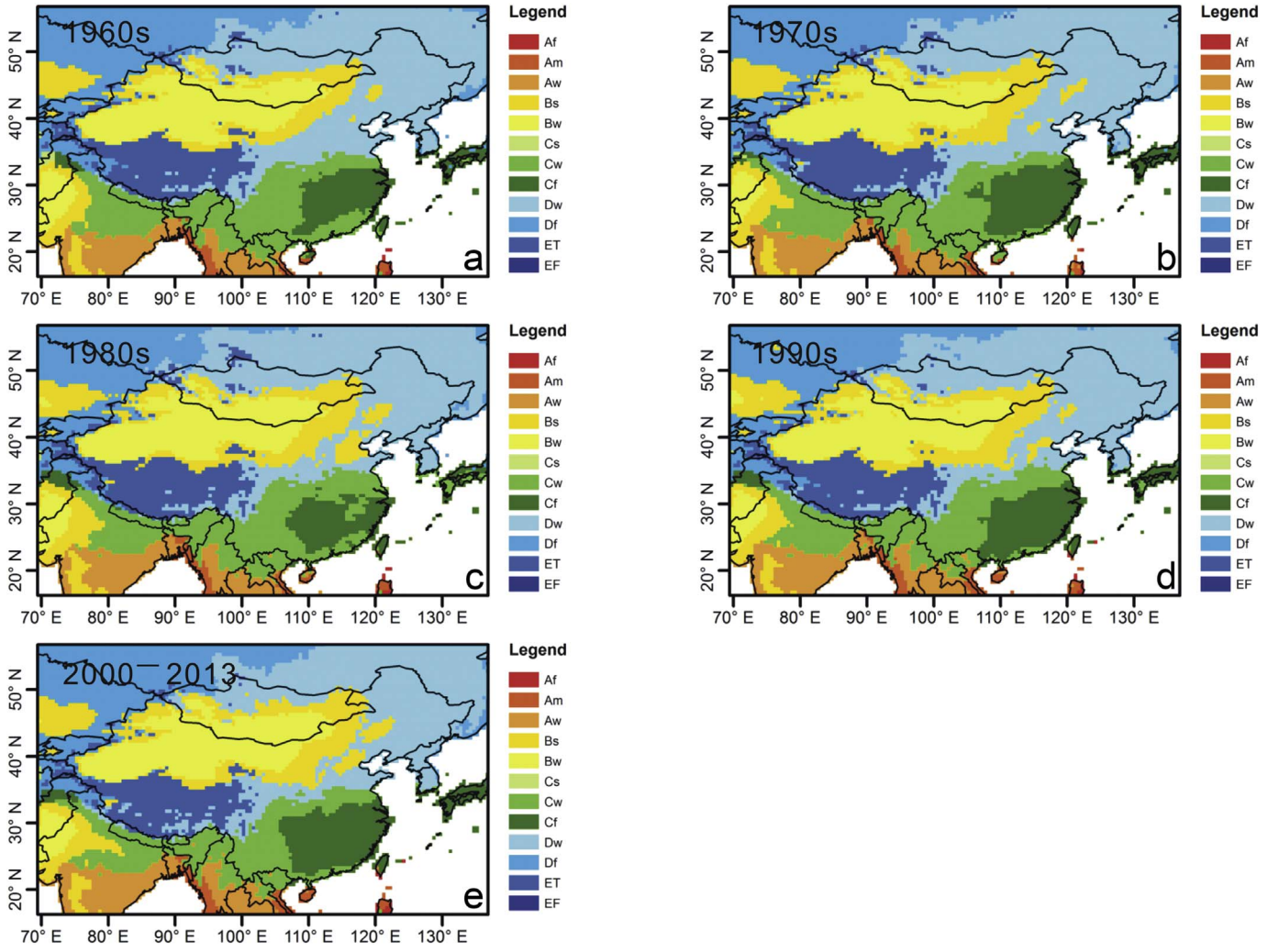

Fig. 5. Changes in Chinese climate zones using Köppen climate classification from 1960s to 2010s.

2.3. Mid-Holocene climate records and lake level simulations in China

Various Holocene climate records have been obtained throughout China to reconstruct long-term paleo-climate variability. We mainly focused on paleo-precipitation and temperature changes during the mid-Holocene. Lake and speleothem records were commonly used to show precipitation variability on millennial and centennial scales. High-resolution and absolutely-dated speleothem records are an good indicator showing Holocene Asian summer monsoon evolution in China (Dykoski et al., 2005; Hu et al., 2008; Cai et al., 2010); however, it is still controversial to explain the cave $\delta^{18}O$ proxy as a monsoon vapor or precipitation proxy (Li et al., 2016). On the contrary, Holocene lake level records in East and Central Asia are closely related to precipitation changes, which have been verified by lake simulations (Li and Morrill, 2010, 2013). Therefore, mid-Holocene lake level records were chosen to reconstruct precipitation change. Mid-Holocene temperature reconstructions were selected from previous publications that directly showed the temperature changes both from lake and ice-core records (Table 2). Holocene lake records in this paper were chosen based on three criteria. (1) The selected lakes must have a reliable chronologies and a successive mid-Holocene sedimentary sequence. (2) The record length should cover the mid-Holocene without documented depositional hiatuses. (3) The indicators derived from the records must include direct lake-level changes or a proxy showing changes in lake depth. Based on the above criteria, twenty-two mid-Holocene lake level records derived from various proxy data were selected (Fig. 2 and Table 2). The radiocarbon ages (^{14}C yr BP) of lakes were calibrated to calendar years (Cal yr BP) by the software of Calib611, if necessary, we removed all possible old-carbon effect using information provided in the original publications. Calibrated ages were used in compiling lake level proxies throughout the text.

The lake-level fluctuation is a highly sensitive indicator for hydrological climate, and many climatic factors, such as precipitation, evaporation and runoff, have direct influence to lake level changes. In order to verify the correlation between mid-Holocene precipitation and lake level records, a series of models, the Community climate system model (CCSM 3.0), a lake energy-balance and a lake water-balance model, were used to simulate Holocene variations in lake-level and examine the reasons for lake-level changes in China between mid-Holocene (ca. 6 ka) and pre-industry (ca. 0 ka). CCSM 3.0 is a state-of-art coupled climate model that consists of four component models of the ocean, sea ice, atmosphere and land that are coupled without flux

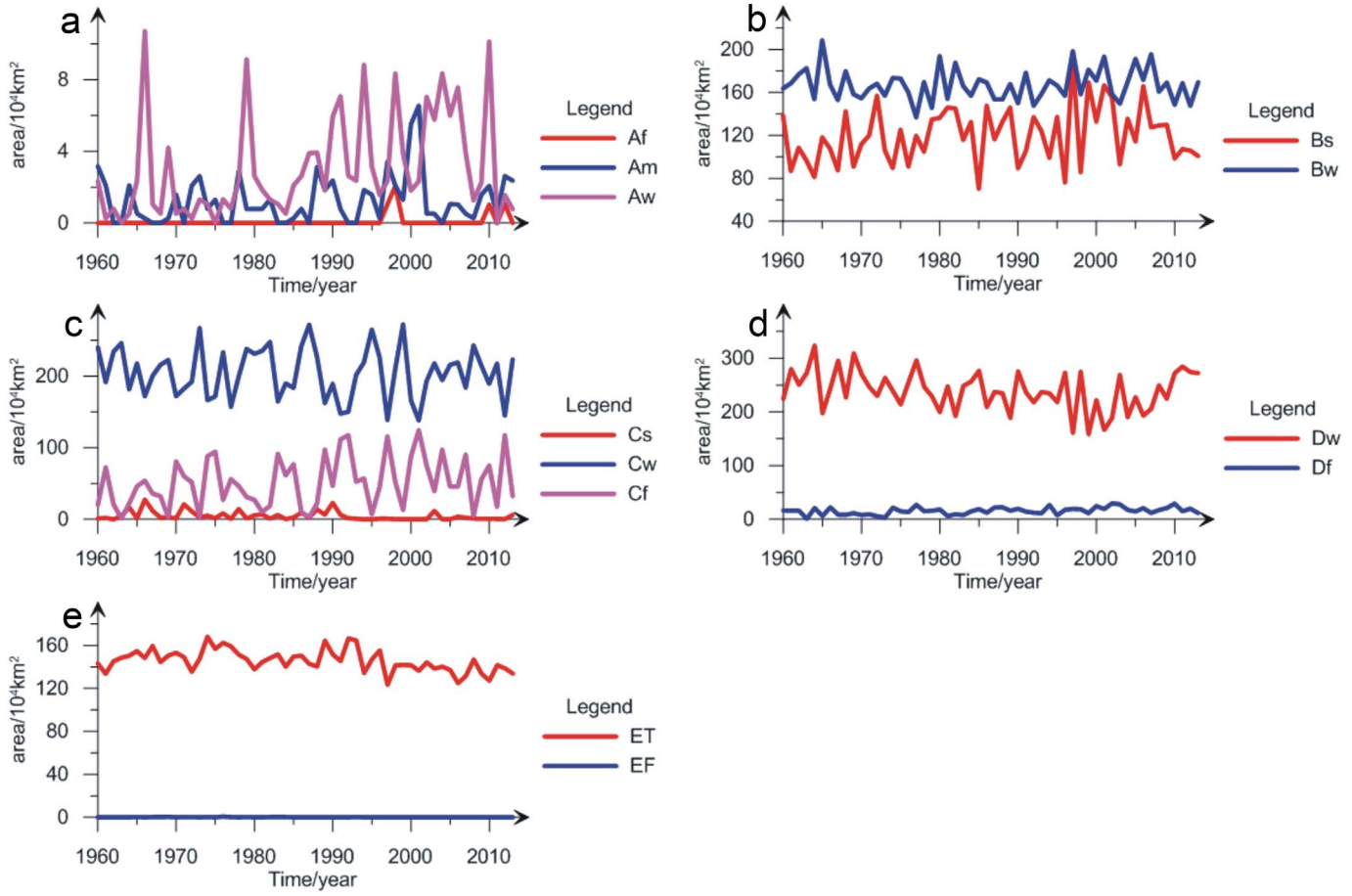

Fig. 6. Variations of Chinese climate zones using Köppen climate classification from 1960s to 2010s.

corrections (Otto-Bliesner et al., 2006). We conducted lake evaporation calculations using a lake energy-balance model that is based on the model of Hostetler and Bartlein (1990). In this model, we assumed the depth of the lake is 1 m and the vertical level of lake water is not mixed. Meanwhile, the surface energy balance for lake is controlled by water surface evaporation. The equation is as follows:

$$c_w \rho_w \frac{\partial T}{\partial t} = \phi_s + \phi_{ld} - \phi_{lu} \pm Q_e \pm Q_h \quad (1)$$

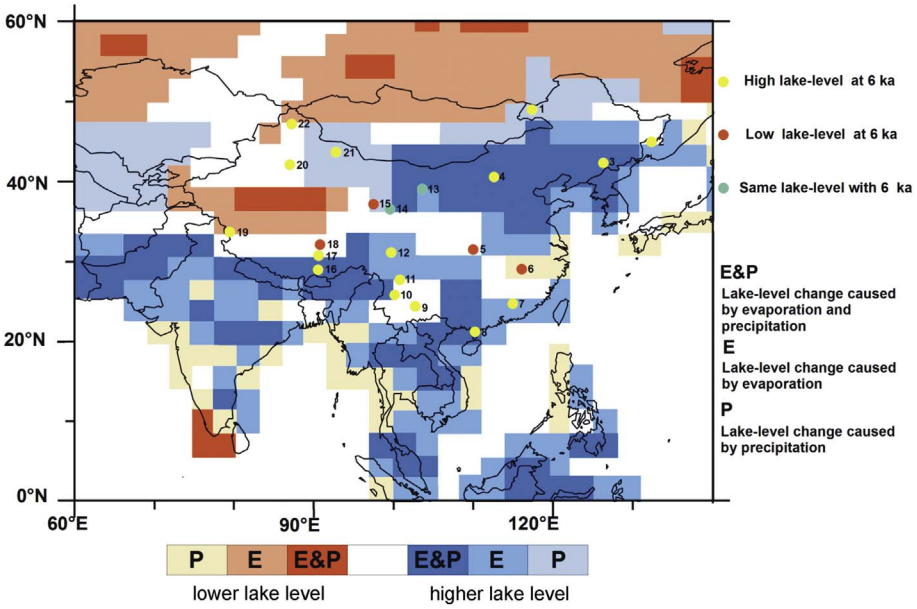

Fig. 7. Results from paleo-lake records and lake level simulations between the mid-Holocene and 0 ka.

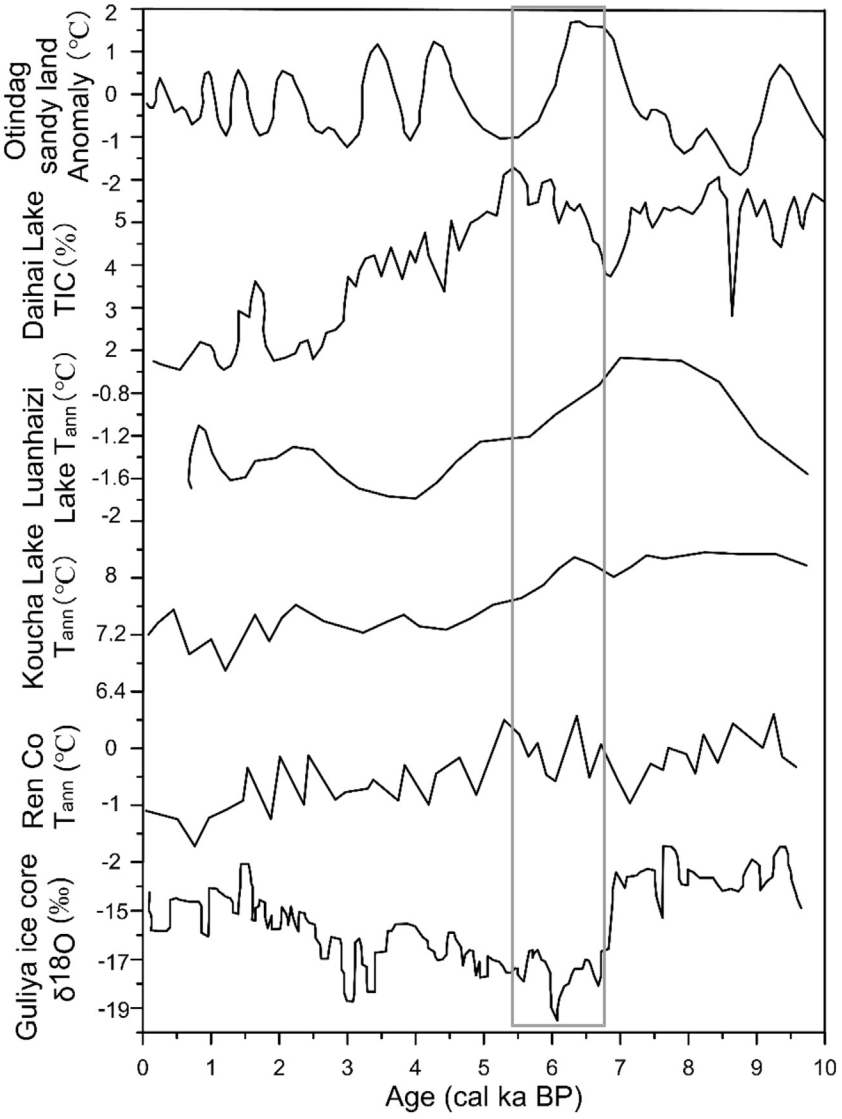
Otindag sandy land Anomaly (°C)
Daihai Lake TIC (%)
Luanhaizi Lake Tann (°C)
Koucha Lake Tann (°C)
Ren Co Tann (°C)
Guliya ice core δ18O (‰)
Age (cal ka BP)

Fig. 8. Variations of Chinese Holocene paleo-temperatures: Daihai Lake (Xiao et al., 2006), Luanhaizi Lake (Herzschuh et al., 2010), Koucha Lake (Herzschuh et al., 2009), Ren Co (Tang et al., 1998), Otindag sandy land (Li et al., 1995), Guliya ice core (He et al., 2003).

where c_w, ρ_w, z and T represent specific heat of water ($J\,kg^{-1}\,K^{-1}$), water density (kg m-3), lake depth (m), and lake surface temperature (K) respectively. T is the time, φ_s and φ_{ld} are shortwave and longwave radiation absorbed by water, φ_{lu} is longwave radiation emitted by lake, Q_e is latent heat fluxes and Q_h is sensible heat fluxes. This paper assumed that each grid cell of the CCSM3 model is a single individual that is in hydrological equilibrium with steady-state conditions of climate, and the lake water-balance equation:

$$V = A_B R + A_L (P_L - E_L) \quad (2)$$

where V is discharge from the lake (m^3/year), A_B and A_L are watershed area (m^2) and lake area (m^2), R is watershed runoff (m/year), P_L is on-lake precipitation (m/year) and E_L is lake evaporation (m/year). Please see Li and Morrill (2010, 2013) for more information about the lake level model parameters.

2.4. PMIP3 and CMIP5 simulations

The Paleoclimate Modeling Intercomparison Project (PMIP) was initiated in order to coordinate and encourage the systematic study of General Circulation Models (GCMs) and to assess their ability to simulate large changes of climate (Joussaume et al., 1999). The mid-Holocene experiment was set up to examine those coupled models' sensitivity to the changes of insolation. Values for precession, obliquity and eccentricity were set according to Berger (1978) and values for greenhouse gases (CO_2, CH_4, and N_2O) were specified following protocols of the PMIP3. Vegetation and other boundary conditions, such as the aerosols, solar constant, ice sheets, topography and coastlines are prescribed as the same as in the Pre-industry (PI, 0 ka) experiments. Ten coupled GCMs from the PMIP3 database are accessed in this study (Table 3). The output data of the PMIP3 mid-Holocene and PI (0 ka) experiments using ten global climate models are available at https://esgf-node.ipsl.fr/esgf-web-fe/. The PMIP3 climatic data were derived from the last 100 yr output for each model. The median values of all PMIP3 models used in this research were considered when evaluating the PMIP3 models simulations. The cubic spline interpolation was applied to interpolating various climate variables on the common 1° × 1° grid and the values of model simulations were then sorted from minimum to maximum in order to extract the median value. A Climatic Research Unit (CRU) updated gridded climate dataset from monthly

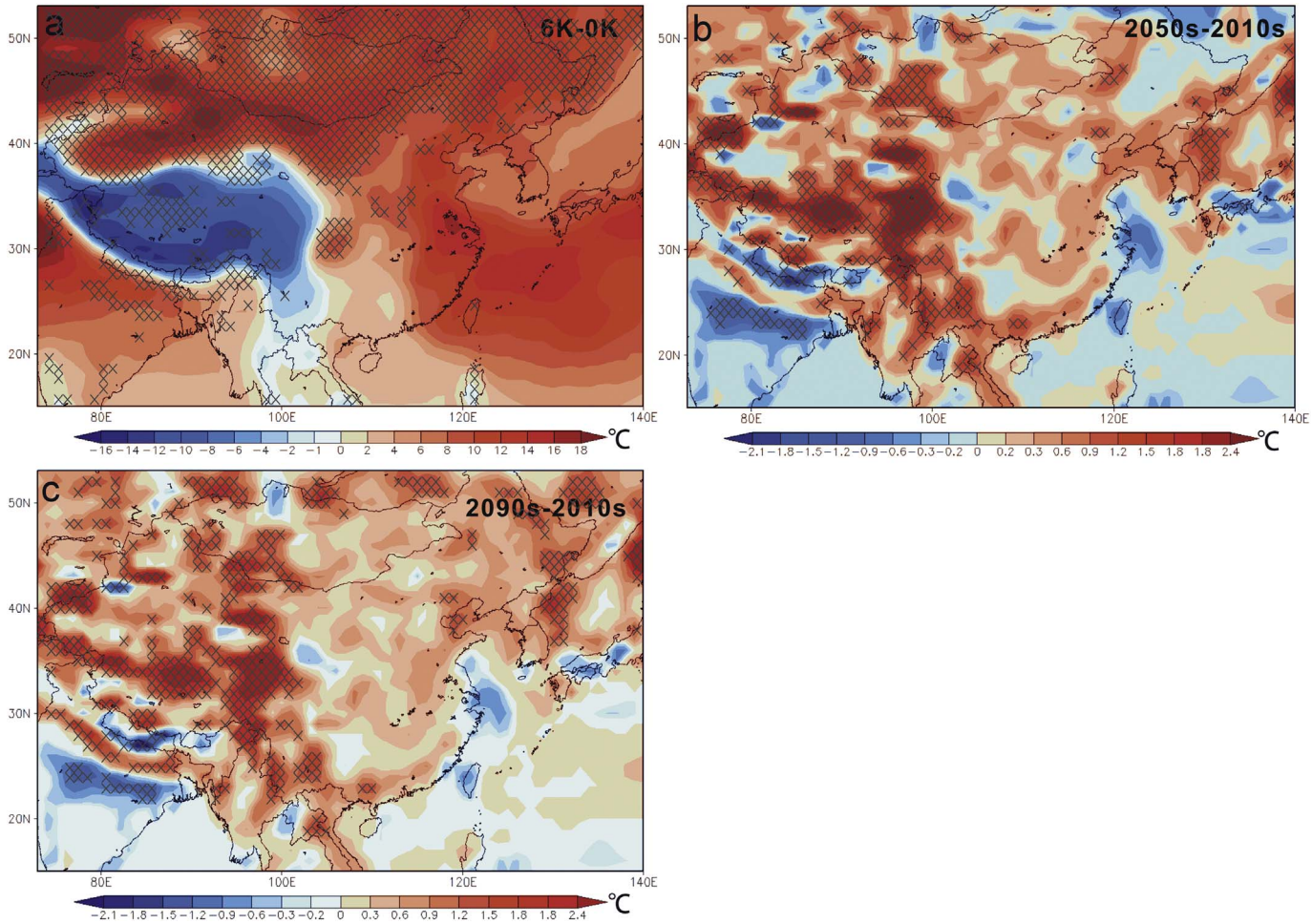

Fig. 9. Difference in summer mean temperature between the mid-Holocene (6 ka) and 0 ka using PMIP3 models, and between 2010s, 2050s and 2090s using CMIP5 models.

observations at meteorological stations across the world's land areas is used to evaluate the Pre-industry (0 ka) simulations of PMIP3 models. The National Centre for Environmental Prediction (NCEP) data are used for the comparison of the monsoon circulations. Fig. 3 shows a comparison between PMIP3 simulated (0 ka) and observed (gridded CRU climate dataset) precipitation and temperature in China, which exhibit a similar pattern between them.

The CMIP5 set of experiments (Taylor et al., 2012) includes simulations of 20th century climate (referred to as historical experiments, 1850 to 2005) and projection experiments (2006 to 2100) of 21st century climate under the new greenhouse gas (GHG) emission scenarios termed “Representative Concentration Pathways” (RCPs, Moss et al., 2010). RCPs represent classes of mitigation scenarios that produce emission pathways following various assumed policy decisions that would influence the time evolution of the future emissions of GHGs, aerosols, ozone, and land use/land cover changes (Moss et al., 2010). The output databases from eight climate models were selected for the climate change projections in China under the RCP 8.5 scenario, which is a continuously rising radiative forcing pathway. Table 4 gives an overview of the associated countries and the resolution of those GCMs. The output data of the CMIP5 projection experiments with RCP 8.5 scenario are available at http://cmip-pcmdi.llnl.gov/cmip5/index.html. All of the data are interpolated by the cubic spline onto a common 1° × 1° grid to obtain the model ensemble and perform the comparison between simulations and observations. The projections on temperature and precipitation under the RCP 8.5 scenario (2010s, 2006–2015; 2050s, 2046–2055; 2090s, 2086–2095) are derived from the median values of the 8 GCMs' outputs.

3. Results

3.1. Modern climate change in China

Linear changes of precipitation and temperature (1960–2013) can show a general trend for climate change in China. As has been shown in Fig. 1, except for the northern Qinghai-Tibet Plateau, China exhibits a warming trend as a whole and warming trends in the southeast and northwest are more severe than those in other regions. Annual mean surface air temperature in China rose by about 0.9–1.3 °C for the last 50 years, with a warming rate of 0.22 °C per 10 years. The warming rate of China in the later half of the 20th century was more rapid than that of the world and the Northern Hemisphere. The warming occurred in winter and spring is more evident than that occurred in summer and autumn, although the warming trend appears in all seasons. According to Chinese geographical divisions, precipitation and temperature trends are shown for various parts of China, including north, south, northwest and the Tibet Plateau (Fig. 4; Zhao, 1983). Temperature changes exhibit similar increasing trends in different regions, but there are large

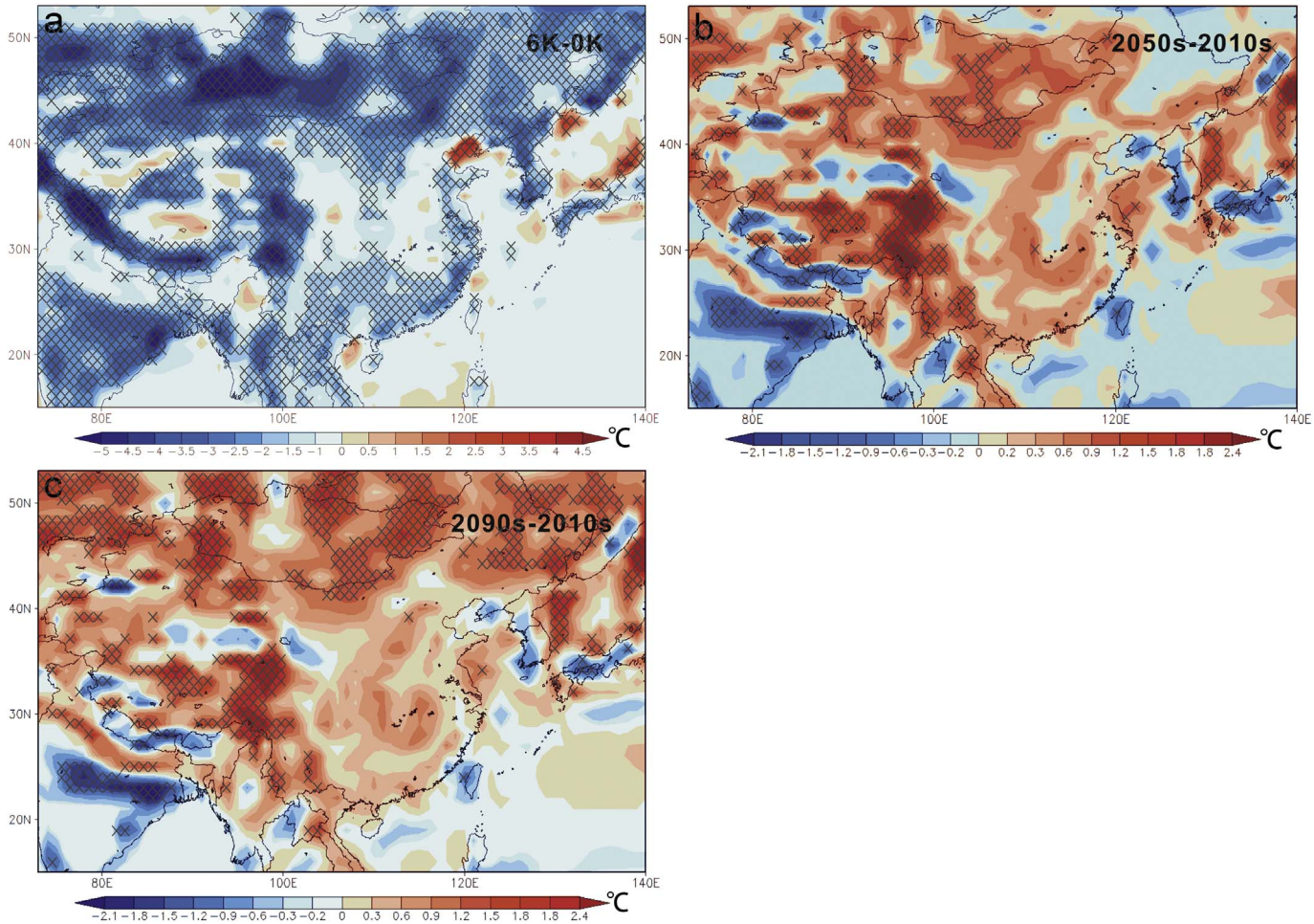

Fig. 10. Difference in winter mean temperature between the mid-Holocene (6 ka) and 0 ka using PMIP3 models, and between 2010s, 2050s and 2090s using CMIP5 models.

differences for annual average temperature at various areas due to different climate zones. Linear trends in precipitation indicate a slowly increasing trend for most parts of China, which becomes more obvious from the northwest to the southeast (Fig. 1). However, the increasing trend cannot be detected clearly in Fig. 4 that illustrates precipitation variability for different regions. Precipitation in southern China varies to a large extent from 1960 to 2013 because of its high annual precipitation. Generally, there is no significant long-term change for annual precipitation in China, a drying interval can be found in the Yellow River Basin and North China Plain especially during 1990–2005. An insignificant wetting trend in most parts of western China and the humid regions in southern China is detectable resulted from a rising in summer rainfall. From 2005, there has been a significant precipitation increase in most parts of China, which is more obvious in northern China than other regions. That is one of the reasons for the positive values of linear precipitation trends from 1960 to 2013.

Fig. 5 shows Chinese climatic zones and their changes from 1960s to 2010s. Köppen climate classification, which is based on temperature and precipitation, has been used to display the impacts of the global warming to climate zones. There are 4 major climate zones, including arid climate (B), warm temperate climate (C) continental climate (D) and polar climates (E) in China. Major climatic types include steppe climate (Bs), desert climate (Bw), warm temperate climate with dry winter (Cw), humid warm temperate climate (Cf), continental climate with dry winter (Dw), humid continental climate (Df) and tundra climate (ET). Decadal climate zone changes are associated with the warming trend in China from 1961 to 2010. The expanding of Bs climate type in Northern China and the eastern part of northwest China is correlated with the drying tendency in this region, and this trend is different from the simple linear precipitation trend that cannot show the decadal scale variability in precipitation. From 1980s to 2010s, areas with the humid temperature (Cf) increase significantly in southern China, which is associated with the wetting trend in that region (Fig. 6). In the Qinghai-Tibet Plateau, areas with dry climate types, Bs and Bw, expand constantly in recently 50 years indicating a decrease in precipitation and an increase in temperature for the north part of the plateau (Fig. 6). Overall, climate zone and type changes in China suggest a drying tendency in the north except for some regions in the northwest and a wetting trend in the south, which are consistent with general changes in precipitation and temperature. However, a wetting tendency has been detected in most of parts of China in recent 10 years (Fig. 6), which is not illustrated clearly by those climate zone maps (Fig. 5).

3.2. Mid-Holocene climate records and simulations

Fig. 7 indicates the lake level change in China between 6 ka and 0 ka, as well as the simulated lake level change between the two periods

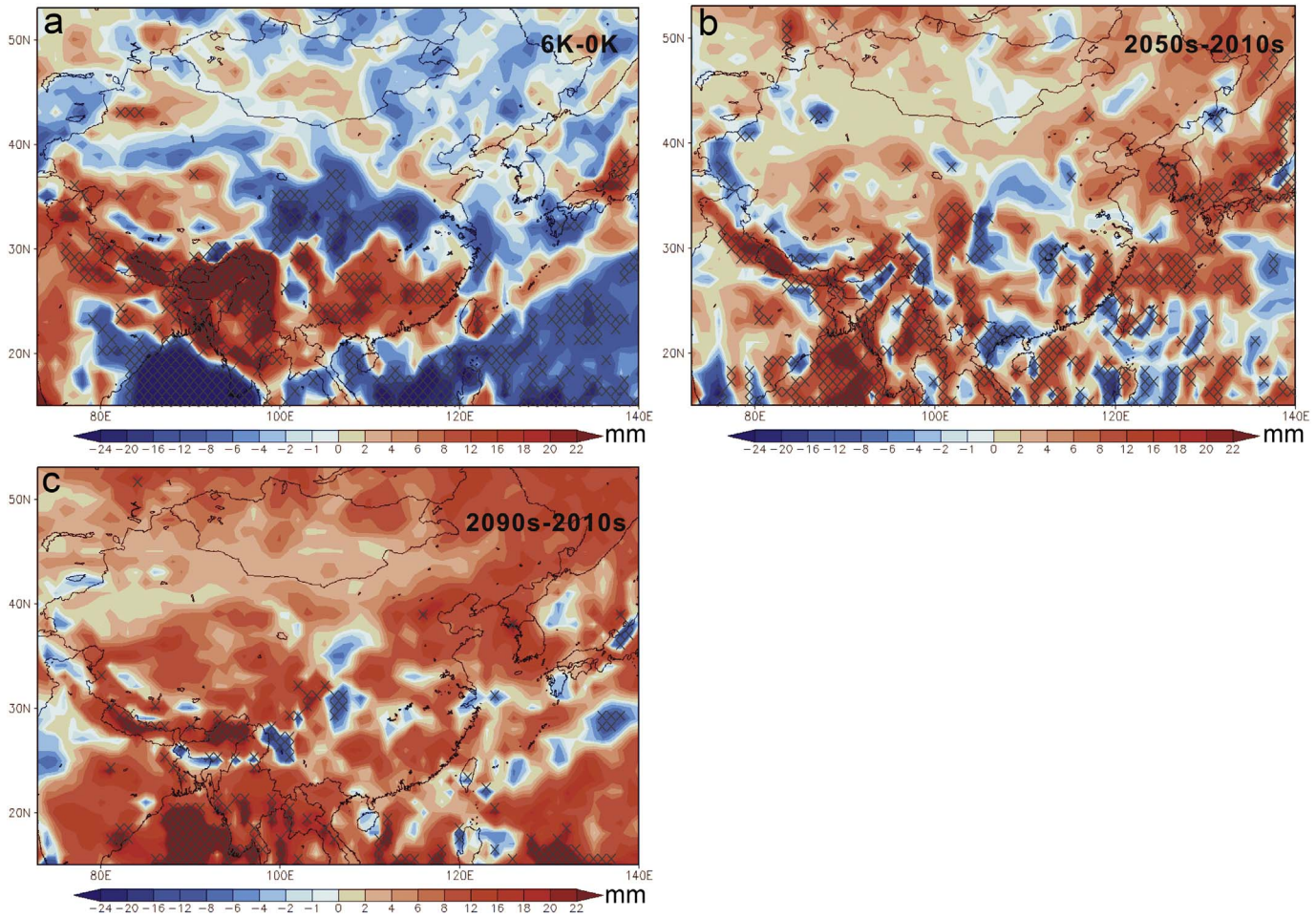

Fig. 11. Difference in monthly mean precipitation between the mid-Holocene (6 ka) and 0 ka using PMIP3 models, and between 2010s, 2050s and 2090s using CMIP5 models.

according to the lake energy & water balance model and CCSM 3. Chinese mid-Holocene lake level records generally show high lake levels relative to 0 ka, except for Zigetang Co and Gaihai Lake in the Qinghai-Tibet Plateau, and Dajiu Lake and Poyang Lake in Eastern China. The simulated lake level change suggests the mid-Holocene low lake level in the northern Qinghai-Tibet Plateau and some areas in southeastern China. Although the simulations and records do not match each other exactly, they show a similar changing pattern. The lake simulations also show the reasons for lake-level changes in China between 6.0 ka and 0 ka (Fig. 7). In monsoonal eastern China, the mid-Holocene high lake level is due to the combined effects of increasing precipitation and decreasing lake evaporation, and evaporation takes a much more important role in some areas of eastern China. In northeastern and northwestern China, the mid Holocene high lake level is maintained by the high precipitation as shown by the lake simulations. The mid-Holocene temperature records were extracted from Daihai Lake (Xiao et al., 2006), Luanhaizi Lake (Herzschuh et al., 2010), Koucha Lake (Herzschuh et al., 2009), Ren Co (Tang et al., 1998), Otindag sandy land (Li et al., 1995), Guliya ice core (He et al., 2003) (Fig. 8). The reconstructed mid-Holocene annual mean temperatures are generally 1–2 °C higher than those of 0 ka except for the relatively low mid-Holocene temperature from the Guliya ice core in the Qinghai-Tibet Plateau. Overall, the compilation from lake level records and simulations, as well as temperature reconstructions, generally shows a warm and humid phase during the mid-Holocene. Low or unchanged mid-Holocene lake levels can be found near the latitude of 30°N, which is related to the strong sub-tropical high in the mid-Holocene that is caused by the high low-latitude insolation and the strong Hadley Circulation, and the low mid-Holocene temperature is detected in the ice core record from the Qinghai-Tibet Plateau.

Figs. 9–13 show temperature and precipitation differences between the mid-Holocene and 0 ka based on median values of PMIP3 models used in this research. In the mid-Holocene the Northern Hemisphere receives more insolation during boreal summer that leads to a significant summer warming over China except for the Qinghai-Tibet Plateau (Fig. 9). The changes of winter temperature show a cooling over most regions of China, especially in the mid-to-high latitudes and some regions in the Qinghai-Tibet Plateau, which is associated with the decreased winter insolation in the NH (Fig. 10). Summer and winter temperature differences suggest that the solar radiation is one of the most important factors that dominate the mid-Holocene temperature in China. The enhanced annual and summer precipitation was observed in the southeast and most parts of northern China, as well as the Qinghai-Tibet Plateau (Figs. 11 and 12) and the summer precipitation increases by 6.89% over Eastern China in the PMIP3. The decreased mid-Holocene winter precipitation is found in most parts of China except for the southernmost region, which is also related to the decreased winter insolation relative to 0 K. Fig. 14 shows changes in Chinese climate zones

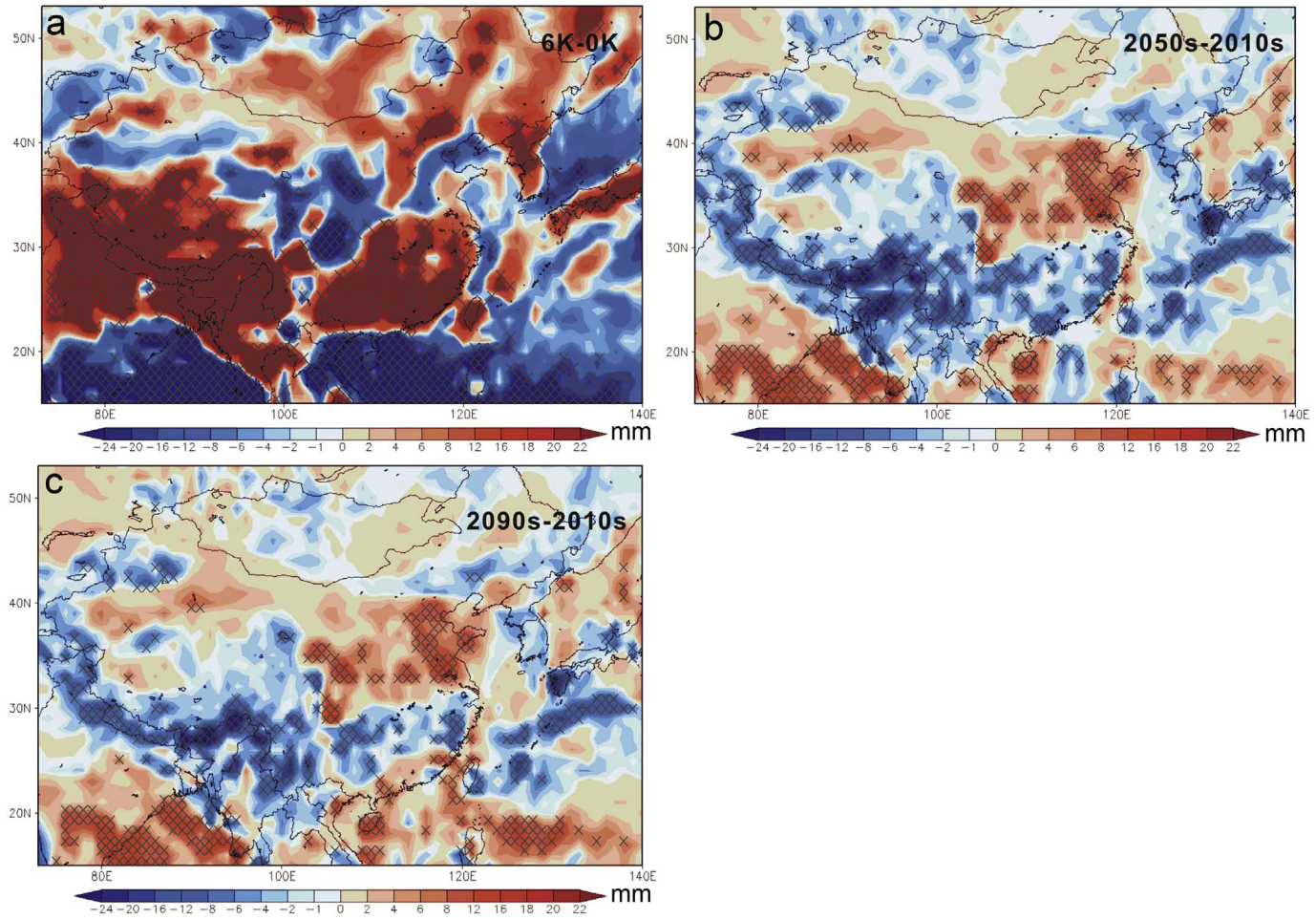

Fig. 12. Difference in monthly mean summer precipitation between the mid-Holocene (6 ka) and 0 ka using PMIP3 models, and between 2010s, 2050s and 2090s using CMIP5 models.

between the mid-Holocene and 0 ka according to median values of PMIP3 models. The most significant changes in climate zones are a decrease in areas of temperate climate with dry winter (Cw) and continental climate with dry winter (Dw) from 6 ka to 0 ka and an increase in areas of humid temperate climate (Cf) and humid continental climate (Df). It shows that fluctuations in precipitation between summer and winter weaken from the mid-Holocene to modern times and highlights the significant difference between winter and summer during the mid-Holocene. As has been shown by PMIP3 models, summer difference in 500 hpa geopotential height between the mid-Holocene and 0 ka generally shows a pattern that is parallel to latitudes suggesting an uniform change in temperature from low to high-latitude regions (Fig. 15). During the winter in the mid-Holocene, the northwest Pacific regions are dominated by a low 500 hpa geopotential height that is high in arid Central Asia. This could trigger strong winter zonal winds at the middle of troposphere in the mid-latitudes (Fig. 16). The mid-Holocene East Asian summer monsoon circulations are strengthened due to the enhanced land-sea thermal contrast during boreal summer (Fig. 12), and the phenomenon was captured by the summer difference in 850 hpa wind fields between the mid-Holocene and 0 ka (Fig. 17). The southerly winds are enhanced significantly in northern China, which emphasizes the mid-Holocene East Asian monsoon impacts. The stronger southerly winds favor the vapor transport from the low to mid-high latitudes that contributes to the enhancement summer precipitation. Strong 850 hpa zonal winds from the mid-latitude Pacific Ocean to northern China are observed according to the winter difference in 850 hpa wind fields, which could be associated with the enhanced land-sea thermal contrast in the mid-Holocene (Fig. 18).

3.3. Human-made global warming

Climate changes in 21st century China are described based on the projections of eight climate models under Representative Concentration Pathway 8.5 (RCP 8.5) scenarios. The results show that warming is expected in all regions of China under the RCP 8.5 scenario, with northern China showing greater warming than southern China, and the warming tendency from 2010s to 2090s is 0.63 °C/10a for RCP8.5. Both summer and winter temperatures exhibit an increasing trend, and the temperature continues to rise with the ongoing increase of radiative forcing (Figs. 9 and 10). The warming in the Tibetan Plateau and the surrounding areas are more obvious in summer than that in winter. The regionally averaged precipitation over China will continue to increase from 2010s to 2090s, and the precipitation increase within the period is 1.8%/10a for RCP8.5. The median precipitation increase from all CMIP5 models for the last 30 years of the 21st century is > 10% for RCP8.5. Figs. 11–13 show the geographical distributions of

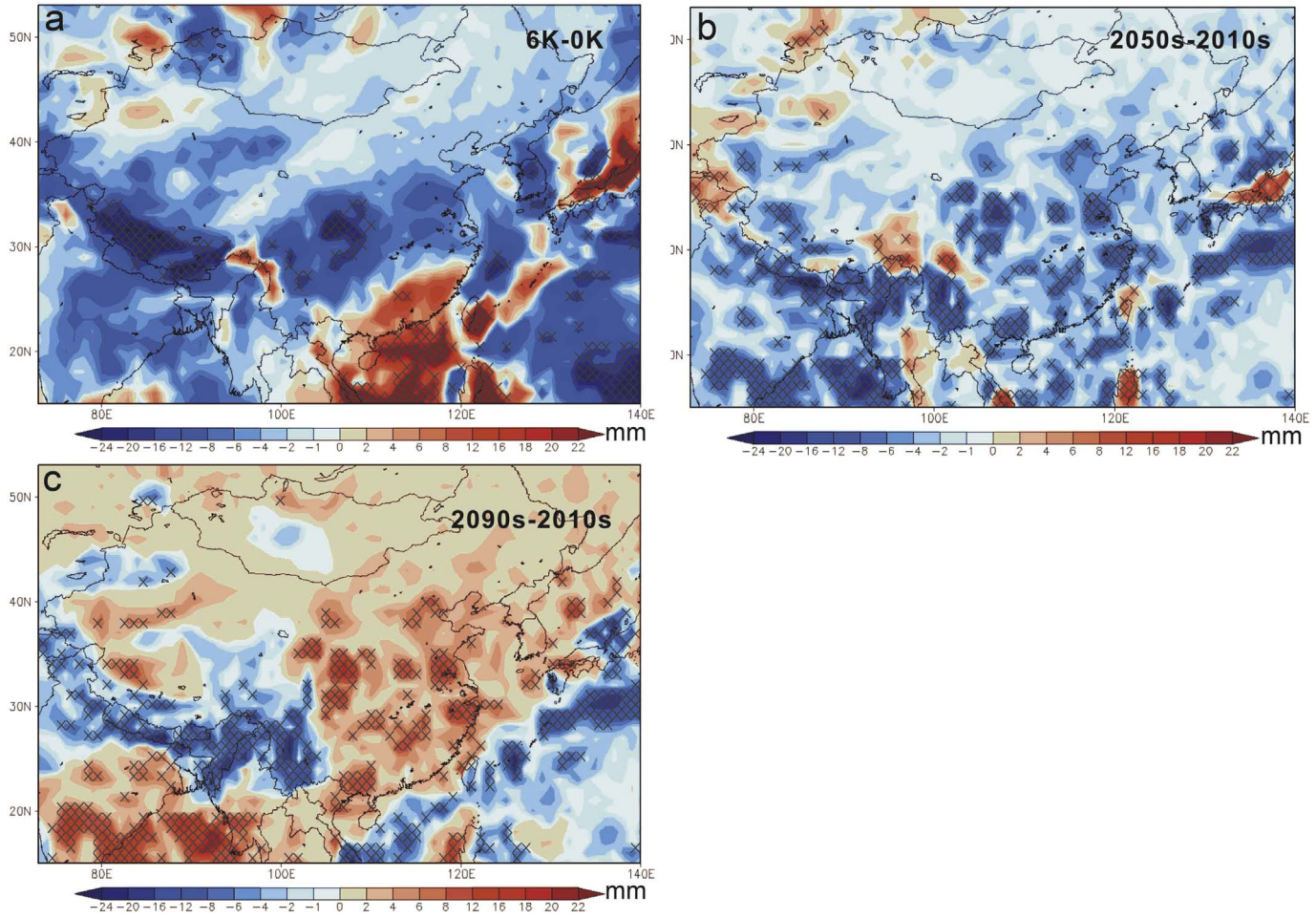

Fig. 13. Difference in monthly mean winter precipitation between the mid-Holocene (6 ka) and 0 ka using PMIP3 models, and between 2010s, 2050s and 2090s using CMIP5 models.

precipitation changes from 2010s to 2090s. The increasing precipitation in northern China is greater than that in the southern regions, and a remarkable increase is found in western and northeastern China, where the changes are statistically significant. However, precipitation change is different for winter and summer season, with continuously increasing summer precipitation from the northern plain and northwest of China. Winter precipitation change is very different between 2010s, 2050s and 2090s, with the most significant winter precipitation increase in

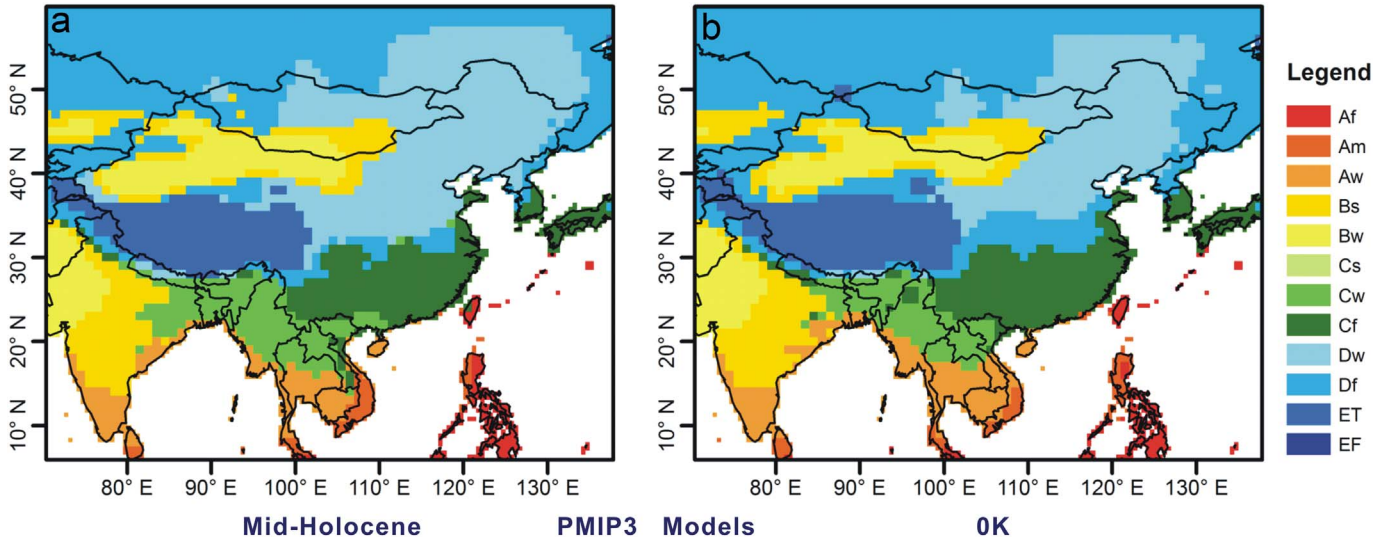

Fig. 14. Chinese climate zones using Köppen climate classification and PMIP3 models in the mid-Holocene (6 ka) and 0 ka.

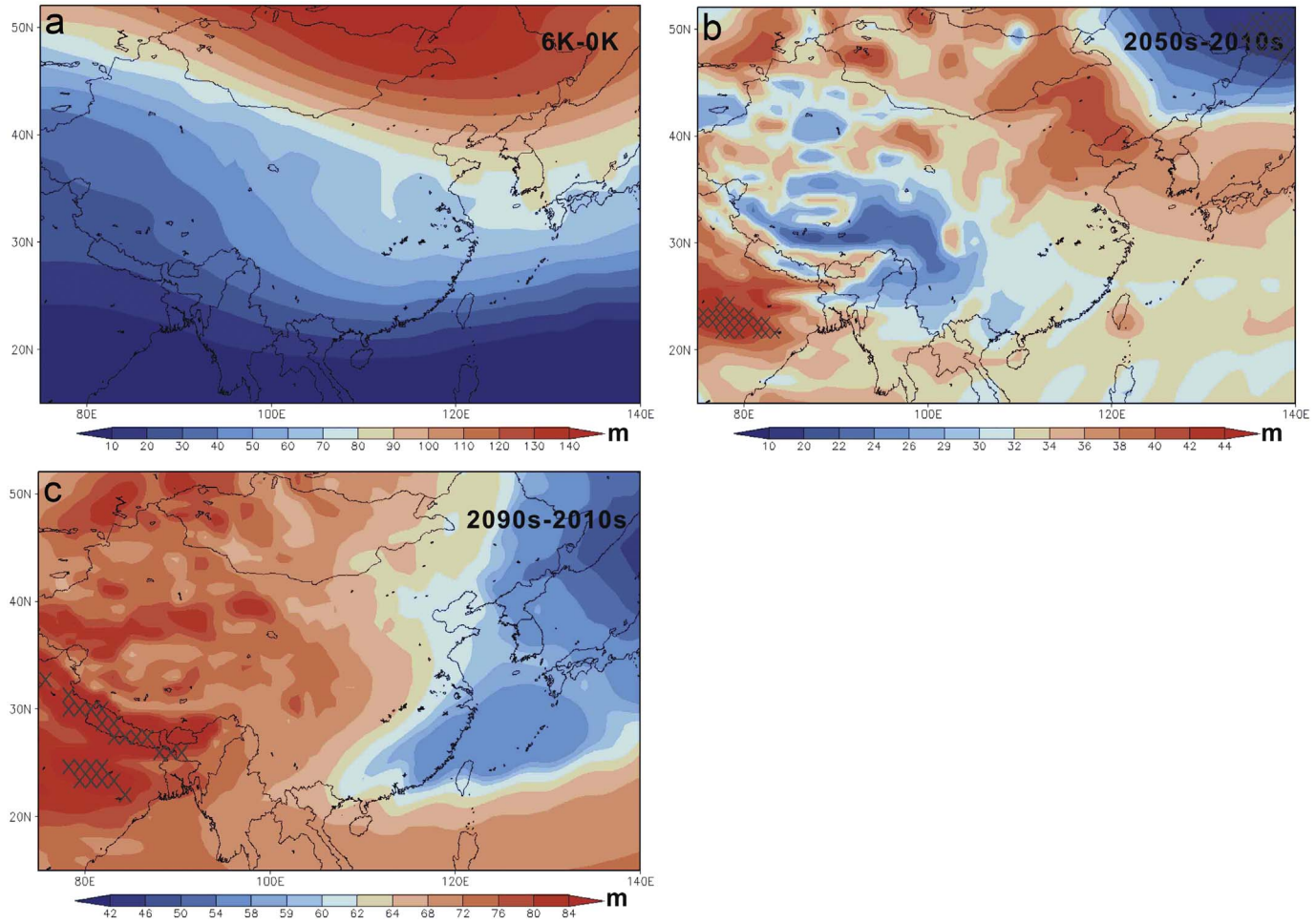

Fig. 15. Difference in monthly mean summer 500 hpa geopotential height field between the mid-Holocene (6 ka) and 0 ka using PMIP3 models, and between 2010s, 2050s and 2090s using CMIP5 models.

southwestern China for the last 10 years of the 21st century. It should be noted that both summer and winter precipitation appears to decrease in southern China for 2050s the RCP 8.5 scenarios.

Fig. 19 shows changes in Chinese climate zones between the 2090s, 2050s and 2010s according to median values of CMIP5 models. Although obvious temperature and precipitation change can be detected through the simulations, it seems changes in climatic factors have few impacts to Chinese climate zones. The 500 hpa geopotential height is generally increasing from 2010s to 2090s over China, but the increasing rate is relatively low for the Qinghai-Tibet Plateau and the northwest of the Pacific Ocean (Figs. 15 and 16). The 500 hpa geopotential height change is closely related to the transform in general circulations and the surface warming, and this pattern in China responds to the inequivalent warming in the Asia Pacific region. The mid-latitude westerlies are intensified in boreal winter from 2010s to 2090s according to difference in 850 hpa wind fields between the 2090s, 2050s and 2010s, suggesting the impacts from the warming of the mid-latitudes (Figs. 17 and 18). The summer 850 hpa zonal winds around 30°N become stronger in the 2050s, and the 850 hpa wind shear affecting newborn cyclone is obvious in the northwest of the Pacific Ocean in the 2090s. There is no regularity in the change of 850 hpa wind fields for other regions of China.

4. Discussion

4.1. Temperature change from the mid-Holocene to the future

Previous proxy data in China have shown the deviation of annual mean temperature between 6 ka and 0 ka, which was roughly estimated at about 1 °C in South China, 2 °C in the Yangtze Valley, 3 °C in North China and Northeast China and the strongest warming by 4–5 °C was recorded in Qinghai-Tibet Plateau (Shi et al., 1993). The results are generally consistent with our synthesis, which has shown a ~0.9 °C increase in temperature in Luanhaizi Lake (Herzschuh et al., 2010), a ~1 °C increase in Koucha Lake (Herzschuh et al., 2009), a ~1.5 °C increase in Ren Co (Tang et al., 1998), a ~2 °C increase in Otindag sandy land (Li et al., 1995) in the mid-Holocene. Our records are mostly located in northern China, and their warming rates are smaller than previous estimates. However, the Guliya ice core record suggests a mid-Holocene low temperature phase, which is different from previous studies (He et al., 2003). According to PMIP3 models, the summer temperature increase in northern and eastern China is between 1 and 2 °C during the middle Holocene, which is similar to our synthesis, but the winter temperature is lower than that of 0 ka over China, especially in northern and western China. This is related to the low mid-Holocene

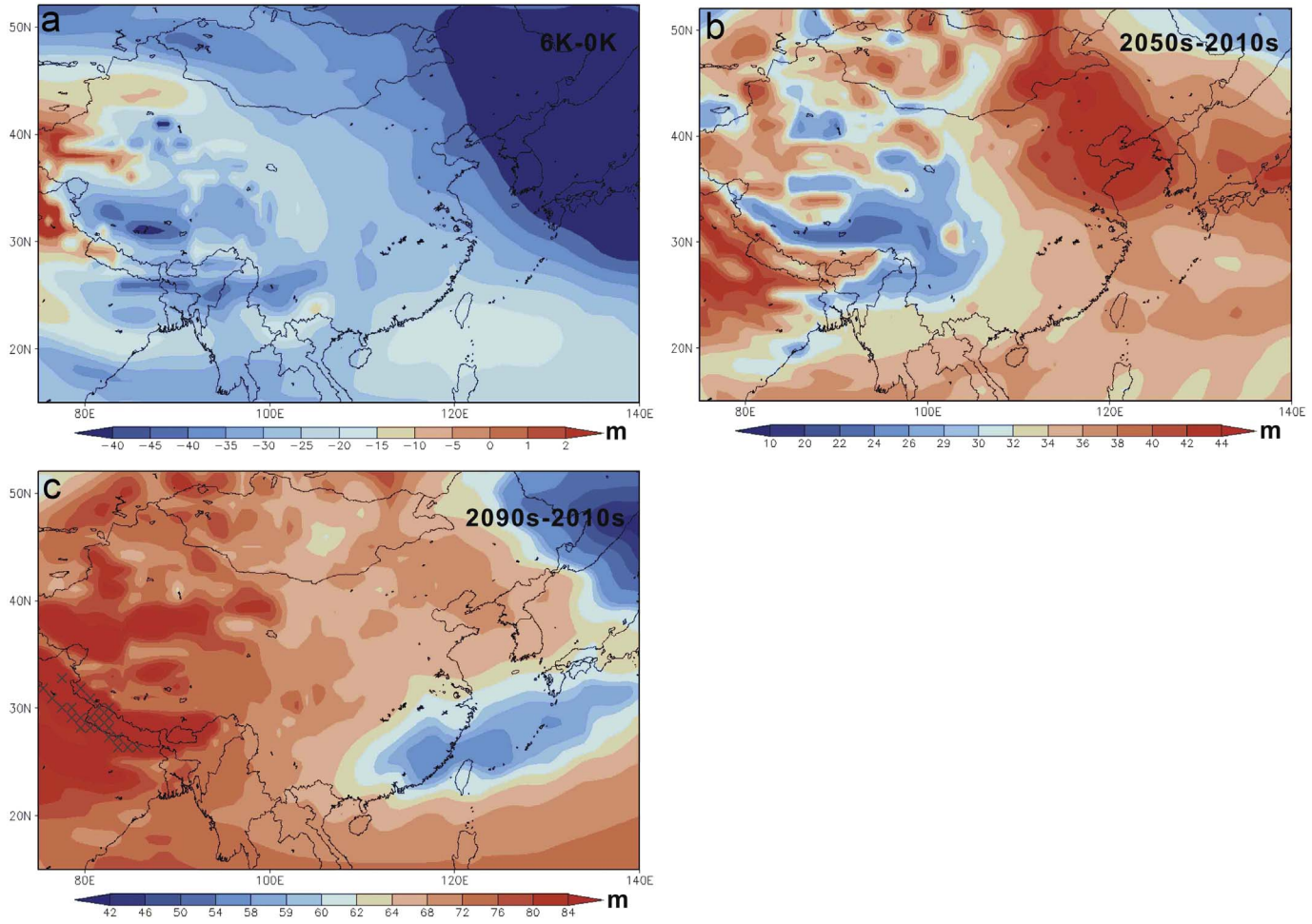

Fig. 16. Difference in monthly mean winter 500 hpa geopotential height field between the mid-Holocene (6 ka) and 0 ka using PMIP3 models, and between 2010s, 2050s and 2090s using CMIP5 models.

winter solar radiation and has been verified by other simulations (Li and Morrill, 2015). Therefore, temperature proxy reconstructions in China are more affected by climatic factors in summer. The Qinghai-Tibet Plateau shows a low mid-Holocene temperature both by PMIP3 simulations and the Guliya ice core record. Further evidence regarding high-resolution records and numerical calculation are needed to investigate this phenomenon.

Third National Assessment of Report on Climate Change of China revealed that average temperatures across China have risen by 0.9 to 1.5 °C from 1909 to 2011 and this trend will further intensify in the future (The Editorial Board of Third National Assessment of Report on Climate Change of China, 2015). Temperatures across China will be substantially higher at 2.7 to 2.9 °C in the 2100s, which is higher than the global goal of containing future temperature increases to an average of 2 °C in this century. The RCP 8.5 scenario of CMIP5 models indicates is a continuously rising radiative forcing pathway. Results from our calculation show both summer and winter warming is found in all China, and the northern regions exhibit greater warming than the southern regions, being especially stronger in the Qinghai-Tibet Plateau, the northern parts of XinJiang, and some areas of the Northeast of China, in accordance with some previous research (Zhou and Yu, 2006; Xu et al., 2009). The naturally-oriented mid-Holocene warming has obvious seasonal difference, which is different from 21st century human-made global warming, and the Qinghai-Tibet Plateau responds them with completely different forms. Moreover, the ~2 °C temperature fluctuation in the 21st century is similar to millennial-scale summer temperature change, which emphasizes the large extent of modern climate change.

4.2. Precipitation change from the mid-Holocene to the future

Mid-Holocene precipitation reconstructions in this synthesis were mainly from Chinese lake level records. Lake levels are commonly affected by many climatic factors such as precipitation and evaporation. Lake level simulations suggest that lake evaporation shows a regionally-coherent pattern that is somewhat more independent of precipitation variations. Lake evaporation is relatively low during the mid-Holocene across nearly all of monsoonal Asia, caused by the strong Asian summer monsoon vapor transport, which can result in high cloud cover. This result is consistent with previous lake evaporation simulations (Li and Morrill, 2010, 2013). At the same time, increased summer monsoon precipitation is synchronous with the decreased lake evaporation, which has been proved by lake level records in monsoonal China. However, regions near the 30°N exhibit almost none lake level changes

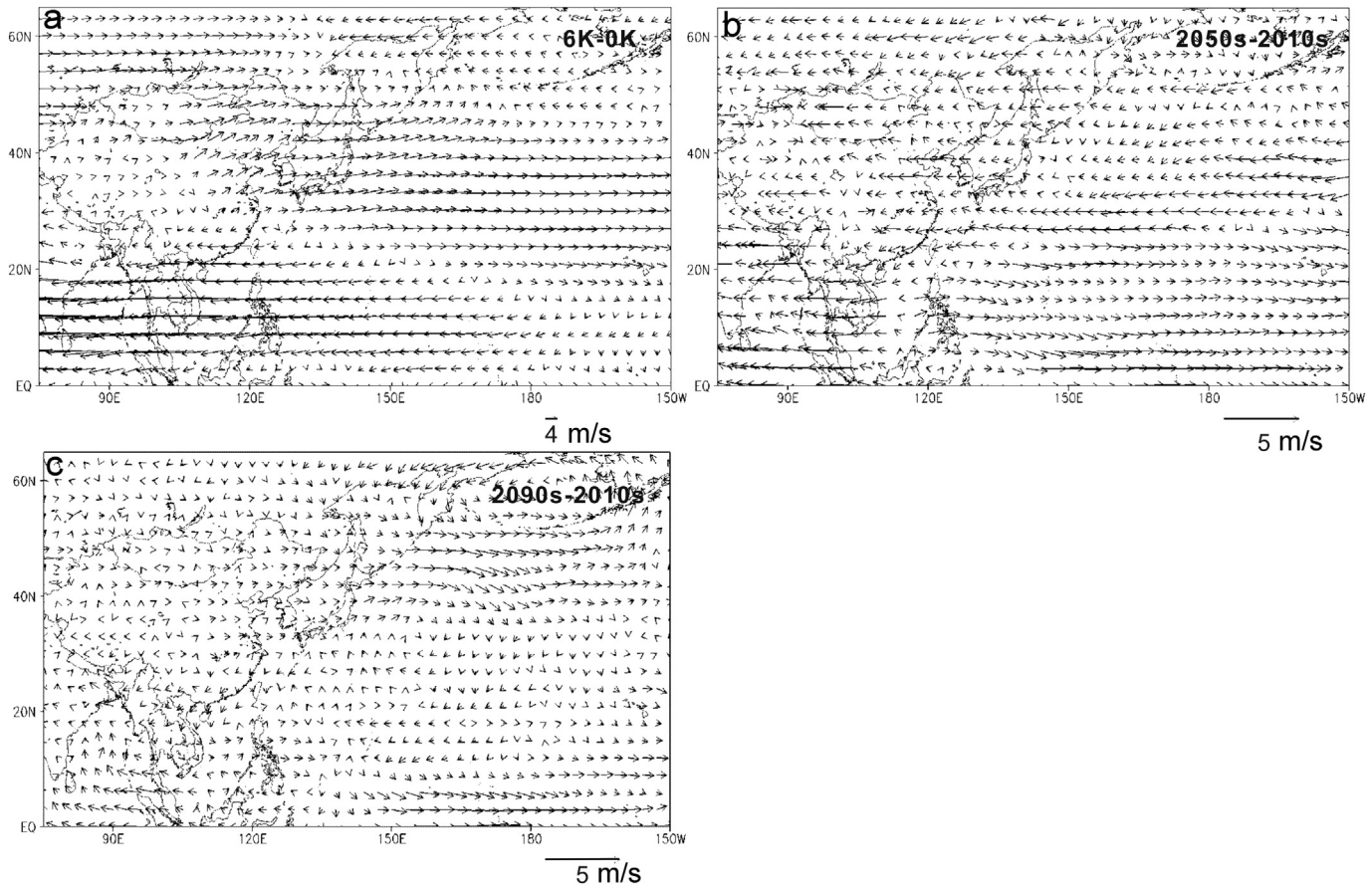

Fig. 17. Difference in monthly mean summer 850 hpa wind field between the mid-Holocene (6 ka) and 0 ka using PMIP3 models, and between 2010s, 2050s and 2090s using CMIP5 models.

or even lower lake levels in the mid-Holocene, and this pattern is recorded by the lake levels from Dajiu Lake (Ma et al., 2008; Zhu et al., 2006) and Poyang Lake (Ma et al., 2004; Jiang and Piperno, 1999) in Eastern China. These regions are usually controlled by the sub-tropical high where the low mid-Holocene summer precipitation is clearly captured by PMIP3 models. Furthermore, simulated mid-Holocene precipitation supports the widely distributed Chinese high lake levels. The reason for the high mid-Holocene lake levels in monsoon marginal zones and arid China is more ascribed to an increase in precipitation other than lake evaporation (Chen et al., 2008; Li and Morrill, 2010).

An et al. (2000) proposed that Holocene Asian summer monsoon precipitation reaches its highest values asynchronously for various Chinese regions. The PMIP3 models do not capture the signals, and the simulated summer precipitation is increased for most parts of China except for the zone near the 30°N. Meanwhile, the decreased mid-Holocene winter precipitation is widely reflected in the simulations, so the discrepancy in Holocene winter and summer precipitation is obvious in the models. Previous PMIP results and Asian summer monsoon simulations approved this general mid-Holocene precipitation pattern (Jiang et al., 2005; Y. Wang et al., 2010; T. Wang et al., 2010; Zheng et al., 2013; Li et al., 2016).

There is a remarkable precipitation change in the 21st century according to CMIP5 models under the 8.5 RCP scenarios. The increasing precipitation in northern China appears greater than that in southern China especially for the summer precipitation. The precipitation in China will continue to increase under the RCP scenarios. The increase rate in annual and seasonal precipitation is accelerated since the 2050s, which marks a threshold of human impacts of precipitation pattern in China. The projection is also verified by previous CMIP5 simulations under RCP2.6, RCP4.5, and RCP8.5 scenarios (Xu and Xu, 2012, H.M. Li et al., 2011; Q. Li et al., 2011). The sub-tropical high has a great impact to Chinese summer precipitation, and the strong mid-Holocene tropical Hadley Circulation intensifies its influence to the zone near the 30°N (Li et al., 2012). The intensified sub-tropical high caused by the mid-Holocene warming is not found in the 21st warming under various simulations (Feng et al., 2010; Xu and Xu, 2012). Compared with other tropical monsoon systems, the East Asian monsoon system is a sub-tropical monsoon, and relationship between precipitation and the sub-tropical high needs further observations and numerical simulations on various time scales.

4.3. Climate zones, 500 hpa geopotential height and 850 hpa wind fields

There is a key projection for changes in future climate zones under human-made global warming in the 21st century, in general, wet areas will become wetter and dry areas drier around the world (Held and Soden, 2006; Seager et al., 2010; Li and Morrill, 2013). This projection is consistent with our research using Köppen climate classification for the last 50 years, in which areas with steppe climate (Bs) and desert climate (Bw) expand constantly in northern China while areas with the

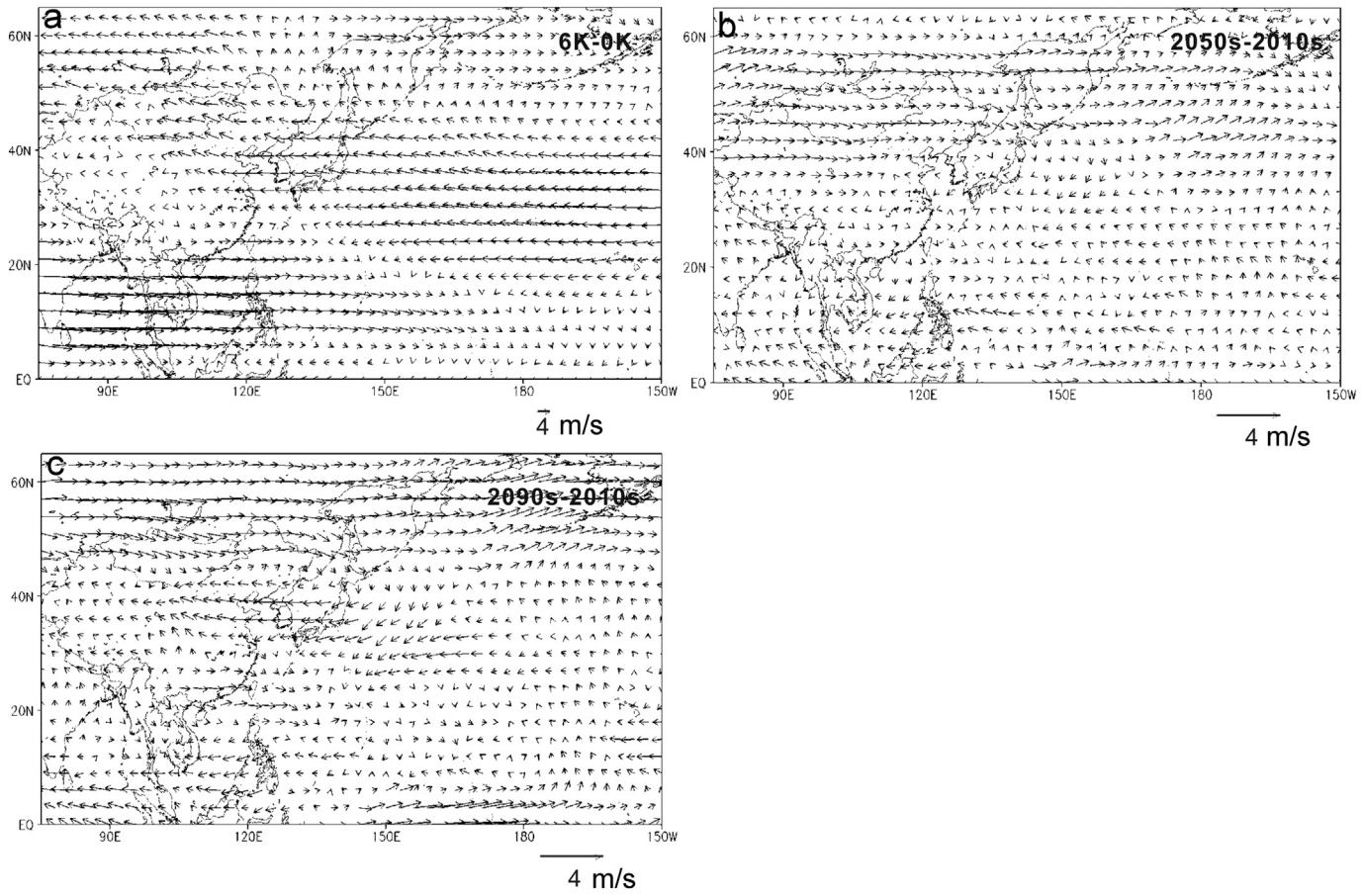

Fig. 18. Difference in monthly mean winter 850 hpa wind field between the mid-Holocene (6 ka) and 0 ka using PMIP3 models, and between 2010s, 2050s and 2090s using CMIP5 models.

humid temperature (Cf) increase significantly in southern China. However, there are no significant changes in climate zones regarding the 21st global warming using CMIP5 models, indicating limited impacts of the warming to climate zones in China. From the mid-Holocene to 0 ka, temperate and continental climate zones with dry winter (Cw and Dw) shrink significantly, which marks the climatic difference between winter and summer weakens. It also suggests the seasonal difference can have greater impacts to Chinese climate zones than the all season warming.

The differences in 500 hpa geopotential height and 850 hpa wind fields demonstrate a different circulation pattern between the naturally oriented warming (the mid-Holocene) and the human-made warming (the 21st century). The mid-Holocene circulation in China is characterized by the strengthened East Asian summer monsoon and the elevated 500 hpa geopotential height paralleled to latitudes, but the human-made global warming is marked by the intensified mid-latitude westerlies and the imbalanced warming tendency between various regions. Our results for the mid-Holocene circulation are consistent with previous PMIP synthesis that emphasized the strengthened African and Asian monsoons due to the amplification of the northern hemisphere seasonal cycle of insolation (Joussaume et al., 1999; Jiang et al., 2005; Y. Wang et al., 2010; T. Wang et al., 2010). The impacts of strong subtropical high, which is highlighted in this study, are also found as a reason for the mid-Holocene summer precipitation decrease in the zone near 30°N (Jiang et al., 2005; Y. Wang et al., 2010; T. Wang et al., 2010). The decreased precipitation is related to the obvious southerly wind anomalies and an anomalous anticyclone over the Northwest Pacific, which could be related to the strengthening and northward migration of the western North Pacific subtropical high (Zheng et al., 2013).

Previous research on CMIP5 models have shown that both the South Asian Summer Monsoon and the East Asian Summer Monsoon were intensified in their climatology under the 21st century warming, featuring increased monsoon precipitation and an enhanced monsoon lower-level westerly jet flow (Sperber et al., 2013; Bao, 2012). Furthermore, the amplitude of the annual and seasonal cycle of rainfall over East Asia is enhanced resulting in a more abrupt monsoon onset (Bao, 2012). The difference analysis in 500 hpa geopotential height and 850 hpa wind fields under the RCP8.5 scenario does not show the intensified summer monsoon in China clearly, since the monsoon strengthening processes are more obvious in the tropical regions and their impacts to northern China are rarely detected in height and wind fields. Most of the wetting trend in northern China is related to the strengthening of the westerlies that is shown in the difference of 850 hpa winds. Therefore, the warming in the mid-Holocene has further enhanced the summer monsoon, and its influence on northern China is much stronger than the modern warming.

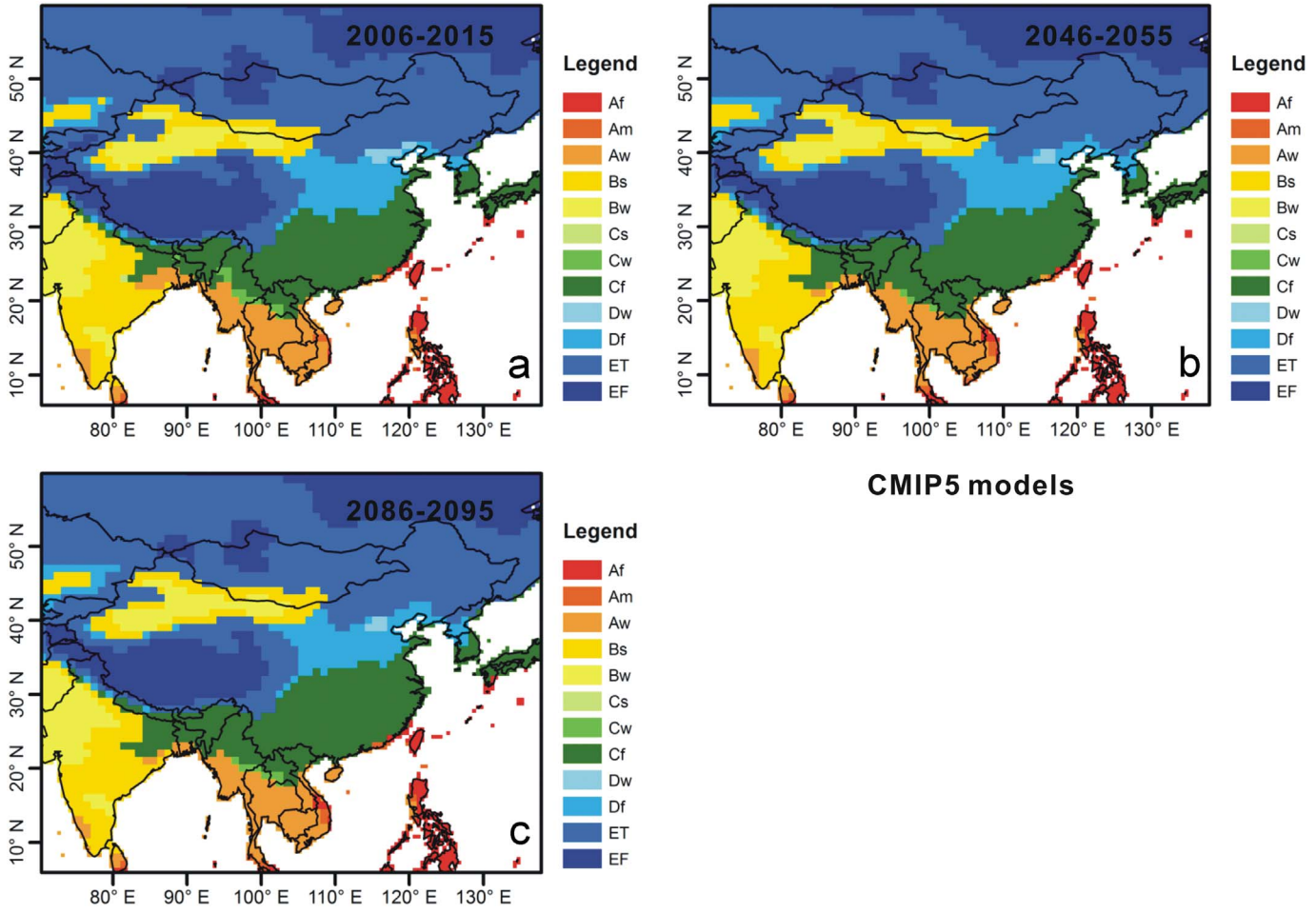

Fig. 19. Chinese climate zones using Köppen climate classification and CMIP5 models in 2010s, 2050s and 2090s.

5. Conclusions

Modern observations, paleo-climate records, CMIP5 (Coupled Model Intercomparison Project Phase 5) and PMIP3 (Paleoclimate Modelling Intercomparison Project 3) simulations, lake level models, numerical climate classification, as well as field analysis of 500 hpa geopotential height and 850 hpa wind were applied to this new approach for the mid-Holocene, modern times and the middle and late periods of the 21st century. Naturally oriented mid-Holocene precipitation and temperature change has significant seasonal signals, which are characterized by warm and humid summer and cold and dry winter. Paleo-lake records that show precipitation/moisture change are relatively consistent with simulations, but paleo-temperature records are more affected by summer temperature. In contrast to few impacts of future global warming to climate classification in China, naturally oriented mid-Holocene period has significant impacts to Chinese climate zones. Temperate and continental dry winter climates expand dramatically during the mid-Holocene warm period. Zonal changes were detected in the 500 hpa geopotential height fields while meridional 850 hpa winds from low latitudes to high latitudes were strengthened for the mid-Holocene. This strengthening was accompanied by a strong Asian summer monsoon. This is no obvious regularity for the impacts of future global warming to 500 hpa geopotential height and 850 hpa wind fields. This study identified manifest difference between naturally oriented and human-made global warming.

Acknowledgements

This work was supported by the National Natural Science Foundation of China (Grant No. 41571178 and 41371009) and the Fundamental Research Funds for the Central Universities (Grant No. lzujbky-2015-143). We thank the editor and reviewers for their constructive suggestions and comments. We acknowledge the modeling groups of CMIP5 and PMIP3 projects.

References

An, Z.S., Porter, S.C., Kutzbach, J.E., Wu, X.H., Wang, S.M., Liu, X.D., Li, X.Q., Zhou, W.J., 2000. Asynchronous Holocene optimum of the East Asian monsoon. Quat. Sci. Rev. 19, 743–762.

Baker, B., Diaz, H., Hargrove, W., 2010. Use of the Köppen-trewartha climate classification to evaluate climatic refugia in statistically derived ecoregions for the People's Republic of China. Clim. Chang. 98, 113–131.

Bao, Q., 2012. Projected changes in Asian summer monsoon in RCP scenarios of CMIP5. Atmos. Oceanic Sci. Lett. 5, 43–48.

Berger, A.L., 1978. Long-term variations of caloric insolation resulting from the Earth's orbital elements. Quat. Res. 9, 139–167.

Cai, Y., Tan, L., Cheng, H., An, Z., Edwards, R.L., Kelly, M.J., Kong, X., Wang, X., 2010. The variation of summer monsoon precipitation in central China since the last deglaciation. Earth Planet. Sci. Lett. 291, 21–31.

Chen, B.S., 2010. Paleoclimate Study Based on High-resolution Sediment Records Since Holocene in Gahai Lake (in Chinese). Doctoral dissertation. Guangzhou University, China.

Chen, F.H., Yu, Z.C., Yang, M.L., Ito, E., Wang, S.M., Madsen, D.B., Huang, X.Z., Zhao, Y., Sato, T., John, H., Birks, B., Boomer, I., Chen, J.H., An, C.B., Wünnemann, B., 2008.

Holocene moisture evolution in arid central Asia and its out–of–phase relationship with Asian monsoon history. Quat. Sci. Rev. 27, 351–364.
Dykoski, C.A., Edwards, R.L., Cheng, H., Yuan, D., Cai, Y., Zhang, M., Lin, Y., Qing, J., An, Z., Revenaugh, J., 2005. A high–resolution, absolute–dated Holocene and deglacial Asian monsoon record from Dongge Cave, China. Earth Planet. Sci. Lett. 233, 71–86.
Fan, H., Gasse, F., Huc, A., Li, Y., Sifeddine, A., Soulié-Märsche, I., 1996. Holocene environmental changes in Bangong Co basin (Western Tibet) Part 3 Biogenic remains. Palaeogeogr. Palaeoclimatol. Palaeoecol. 120, 65–78.
Feng, L., Zhou, T.J., Wu, B., et al., 2010. Projection of future precipitation change over China with a high-resolution global atmospheric model. Adv. Atmos. Sci. 28, 464–476.
Hansen, J., Ruedy, R., Sato, M., Lo, K., 2010. Global surface temperature change. Rev. Geophys. 48, RG4004. http://dx.doi.org/10.1029/2010RG000345.
He, Y., Theakstone, W.H., Zhang, Z.L., Zhang, D., Yao, T.D., Chen, T., Shen, Y.P., Pan, H.X., 2004. Asynchronous Holocene climate change across China. Quat. Res. 61, 52–63.
Harris, I., Jones, P.D., Osborn, T.J., Lister, D.H., 2013. Updated high-resolution grids of monthly climatic observations – the CRU TS3.10 Dataset. Int. J. Climatol. 34, 623–642.
Held, I.M., Soden, B.J., 2006. Robust responses of the hydrological cycle to global warming. J. Clim. 19, 5686–5699.
Herzschuh, U., 2006. Palaeo–moisture evolution in monsoonal Central Asia during the last 50,000 years. Quat. Sci. Rev. 25, 163–178.
Herzschuh, U., Kramer, A., Mischke, S., Zhang, C., 2009. Quantitative climate and vegetation trends since the late glacial on the northeastern Tibetan plateau deduced from Koucha lake pollen spectra. Quat. Res. 71, 162–171.
Herzschuh, U., Birks, H.J.B., Mischke, S., Zhang, C., Böhner, J., 2010. A modern pollen–climate calibration set based on lake sediments from the Tibetan plateau and its application to a late Quaternary pollen record from the Qilian mountains. J. Biogeogr. 37, 752–766.
Hodell, D.A., Brenner, M., Kanfoush, S.L., Curtis, J.H., Stoner, J.S., Whitmore, T.J., 1999. Paleoclimate of southwestern China for the past 50,000 yr inferred from lake sediment records. Quat. Res. 1999, 369–380.
Hostetler, S.W., Bartlein, P.J., 1990. Simulation of lake evaporation with application to modeling lake level variations of HarneyeMalheur Lake, Oregon. Water Resour. Res. 26, 2603–2612.
Hu, C., Henderson, G.M., Huang, J., Xie, S., Sun, Y., Johnson, K.R., 2008. Quantification of Holocene Asian monsoon rainfall from spatially separated cave records. Earth Planet. Sci. Lett. 266, 221–232.
Jiang, Q.H., Piperno, D.R., 1999. Environmental and archaeological implications of a late Quaternary palynological sequence, Poyang Lake, southern China. Quat. Res. 52, 250–258.
Jiang, D.B., Wang, H.J., Lang, X.M., 2005. Evaluation of East Asian climatology as simulated by seven coupled models. Adv. Atmos. Sci. 22, 479–495.
Jiang, Q., Shen, J., Liu, X., Zhang, E., Xiao, X., 2007. A high-resolution climatic change since Holocene inferred from multi-proxy of lake sediment in westerly area of China. Chin. Sci. Bull. 52, 1970–1979.
Jones, P.D., Wigley, T.M.L., 2010. Estimation of global temperature trends: What's important and what isn't. Clim. Chang. 100, 59–69.
Joussaume, S., Taylor, K.E., Braconnot, P., Mitchell, J.F.B., Kutzbach, J.E., Harrison, S.P., Prentice, I.C., Broccoli, A.J., Abe-Ouchi, A., Bartlein, P.J., Bonfils, C., Dong, B., Guiot, J., Herterich, K., Hewitt, C.D., Jolly, D., Kim, J.W., Kislov, A., Kitoh, A., Loutre, M.F., Masson, V., McAvaney, B., McFarlane, N., de Noblet, N., Peltier, W.R., Peterschmitt, J.Y., Pollard, D., Rind, D., Royer, J.F., Schlesinger, M.E., Syktus, J., Thompson, S., Valdes, P., Vettoretti, G., Webb, R.S., Wyputta, U., 1999. Monsoon changes for 6000 years ago: results of 18 simulations from the paleoclimate modeling Intercomparison project (PMIP). Geophys. Res. Lett. 26, 859–862.
Kerwin, M., Overpeck, J.T., Webb, R.S., DeVernal, A., Rind, D.H., Healy, R.J., 1999. The role of oceanic forcing in mid-Holocene northern hemisphere climatic change. Paleoceanography 14, 200–210.
Kramer, A., Herzschuh, U., Mischke, S., Zhang, C., 2010. Holocene treeline shifts and monsoon variability in the Hengduan Mountains (southeastern Tibetan Plateau), implications from palynological investigations. Palaeogeogr. Palaeoclimatol. Palaeoecol. 286, 23–41.
Kramer, A., Herzschuh, U., Mischke, S., Zhang, C., 2010. Late Quaternary environmental history of the south-eastern Tibetan Plateau inferred from the Lake Naleng non-pollen palynomorph record. Veg. Hist. Archaeobotany 19, 453–468.
Li, Y., Morrill, C., 2010. Multiple factors causing Holocene lake-level change in monsoonal and arid central Asia as identified by model experiments. Clim. Dyn. 35, 1115–1128.
Li, Y., Morrill, C., 2013. Lake levels in Asia at the Last Glacial Maximum as indicators of hydrologic sensitivity to greenhouse gas concentrations. Quat. Sci. Rev. 60, 1–12.
Li, Y., Morrill, C., 2015. A Holocene East Asian winter monsoon record at the southern edge of the Gobi Desert and its comparison with a transient simulation. Clim. Dyn. 45, 1219–1234.
Li, S., Sun, W., Li, X.Z., 1995. Sedimentary characteristics and environmental evolution of Otindag sandy land in Holocene (in Chinese). J. Desert Res. 15, 323–331.
Li, S.J., Wünnemann, B., Xia, W.L., 2009. A preliminary study of the Holocene lake level changes and their causes derived from the sediment record of Zigetang Lake, Tibetan Plateau. 16. Earth Science Frontiers, pp. 162–167.
Li, Y., Wang, N., Cheng, H., Long, H., Zhao, Q., 2009. Holocene environmental change in the marginal area of the Asian monsoon a record from Lake Zhuye, NW China. Boreas 38, 349–361.
Li, H.M., Feng, L., Zhou, T.J., 2011. Multi-model projection of July–August climate extreme changes over China under CO2 doubling. Part I: precipitation. Adv. Atmos. Sci. 28, 433–447.
Li, Q., Lu, H., Zhu, L., Wu, N., Wang, J., Lu, X., 2011. Pollen-inferred climate changes and vertical shifts of alpine vegetation belts on the northern slope of the Nyainqentanglha Mountains (central Tibetan Plateau) since 8.4 kyr BP. The Holocene 21, 939–950.
Li, Y., Wang, N., Chen, H., Li, Z., Zhou, X., Zhang, C., 2012. Tracking millennial-scale climate change by analysis of the modern summer precipitation in the marginal regions of the Asian monsoon. J. Asian Earth Sci. 58, 78–87.
Li, Y., Wang, N., Zhou, X., Zhang, C., Wang, Y., 2014. Synchronous or asynchronous Holocene Indian and East Asian summer monsoon evolution: a synthesis on Holocene Asian summer monsoon simulations, records and modern monsoon indices. Glob. Planet. Chang. 116, 30–40.
Li, Y., Zhang, C., Wang, Y., 2016. The verification of millennial-scale monsoon water vapor transport channel in northwest China. J. Hydrol. 536, 273–283.
Liu, Q., Gu, Z., Liu, J., You, H., Lu, H., Chu, G., Georg, S., 2005. Bulk organic carbon isotopic record of Huguangyan Maar Lake, Southeastern China and its paleoclimatic and paleoenvironmental significance since 62 kaBP (in Chinese). Mar. Geol. Quat. Geol. 25, 115–126.
Liu, X., Herzschuh, U., Shen, J., Jiang, Q., Xiao, X., 2008. Holocene environmental and climatic changes inferred from Wulungu Lake in northern Xinjiang, China. Quat. Res. 70, 412–425.
Liu, Y.Y., Zhang, S.Q., Liu, J.Q., You, H.T., Han, J.T., 2008. Vegetation and environment history of Erlongwan Maar Lake during the late Pleistocene on pollen record (in Chinese). Acta Microbiol Sin. 25, 274–280.
Ma, Z.X., Huang, J.H., Wei, Y., Li, J.H., Hu, C.Y., 2004. Organic carbon isotope records of the Poyang Lake sediments and their implications for the paleoclimate during the last 8 ka (in Chinese). Geochimica 33, 279–285.
Ma, C., Zhu, C., Zheng, C., Wu, C., Guan, Y., Zhao, Z., Huang, R., 2008. High-resolution geochemistry records of climate changes since late-glacial from Dajiuhu peat in Shennongjia Mountains, Central China (in Chinese). Chin. Sci. Bull. 53, 28–39.
Marcott, S.A., Shakun, J.D., Clark, P.U., Mix, A.C., 2013. A reconstruction of regional and global temperature for the past 11,300 years. Science 339, 1198–1201.
Mingram, J., Schettler, G., Nowaczyk, N., Luo, X., Lu, H., Liu, J., Negendank, J.F., 2004. The Huguang Maar lake—a high-resolution record of palaeoenvironmental and palaeoclimatic changes over the last 78,000 years from South China. Quat. Int. 122, 85–107.
Moss, R., Edmonds, J., Hibbard, K., 2010. The next generation of scenarios for climate change research and assessment. Nature 463, 747–756.
Otto-Bliesner, B.L., Brady, E.C., Clauzet, G., Tomas, R., Levis, S., Kothavala, Z., 2006. Last glacial maximum and Holocene climate in CCSM3. J. Clim. 19, 2526–2544.
Peel, M.C., Finlayson, B.L., Mcmahon, T.A., 2007. Updated world map of the Köppen-Geiger climate classification. Hydrol. Earth Syst. Sci. 4, 439–473.
PAGES Scientific Steering Committee, 2009. Science Plan and Implementation Strategy. IGBP Report No. 57, IGBP.
Seager, R., Naik, N., Vecchi, G.A., 2010. Thermodynamic and dynamic mechanisms for large-scale changes in the hydrologic cycle in response to global warming. J. Clim. 23, 4651–4668.
Shen, J., Liu, X., Ryo, M., Wang, S., Yang, X., 2004. A high-resolution climatic change since the Late Glacial Age inferred from multi-proxy of sediments in Qinghai Lake. Sci. China Earth Sci. 34, 582–589.
Shen, J., Liu, X.Q., Wang, S.M., Matsumoto, R., 2005. Palaeoclimatic changes in the Qinghai Lake area during the last 18,000 years. Quat. Int. 136, 131–140.
Shen, J., Yang, L., Yang, X., Matsumoto, R., Tong, G., Zhu, Y., Wang, S., 2005. Lake sediment records on climate change and human activities since the Holocene in Erhai catchment, Yunnan Province, China. Sci. China Earth Sci. 48, 353–363.
Shen, J., Jones, R.T., Yang, X., Dearing, J.A., Wang, S., 2006. The Holocene vegetation history of Lake Erhai, Yunnan province southwestern China the role of climate and human forcings. The Holocene 16, 265–276.
Shi, Y., Kong, Z., Wang, S., Tang, L., Wang, F., Yao, T., Zhao, X., Zhang, P., Shi, S., 1993. Mid-holocene climates and environments in China. Glob. Planet. Chang. 7, 219–233.
Sperber, K.R., Annamalai, H., Kang, I.S., Kitoh, A., Moise, A., Turner, A., Wang, B., Zhou, T., 2013. The Asian summer monsoon: an intercomparison of CMIP5 vs. CMIP3 simulations of the late 20th century. Clim. Dyn. 41, 2711–2744.
Tang, L.Y., Shen, C.M., Kong, Z.Z., Wang, F.B., Liu, K.B., 1998. Pollen evidence of climate during the last glacial maximum in Eastern Tibetan Plateau (in Chinese). J. Glaciol. Geocryol. 20, 133–140.
Tao, S.C., An, C.B., Chen, F.H., 2010. Holocene vegetation changes interpreted from pollen records in Balikun Lake, Xinjiang, China (in Chinese). Acta Palaeontol. Sin. 48, 194–199.
Taylor, K.E., Stouffer, R.J., Meehl, G.A., 2012. An overview of CMIP5 and the experiment design. Bull. Am. Meteorol. Soc. 934, 485–498.
The Editorial Board of the Third National Assessment of Report on Climate Change, 2015. Third National Assessment of Report on Climate Change. Science Press, Beijing.
Van Campo, E., Cour, P., Hang, S., 1996. Holocene environmental changes in Bangong co basin (Western Tibet) part 2 the pollen record. Palaeogeogr. Palaeoclimatol. Palaeoecol. 120, 49–63.
Wang, SM., Ji, L., 1995. Sedimentology of late Quaternary lacustrine deposits and history of lake level fluctuation in Hulun lake. J. Lake Sci. 7, 297–306.

Wang, S.W., Gong, D.Y., 2000. Enhancement of the warming trend in China. Geophys. Res. Lett. 27, 2581–2584.
Wang, B., Lin, H., 2002. Rainy season of the Asian–Pacific summer monsoon. J. Clim. 15, 386–396.
Wang, Y., Liu, X., Herzschuh, U., 2010. Asynchronous evolution of the Indian and East Asian Summer Monsoon indicated by Holocene moisture patterns in monsoonal central Asia. Earth Sci. Rev. 103, 135–153.
Wang, T., Wang, H.J., Jiang, D.B., 2010. Mid-Holocene East Asian summer climate as simulated by the PMIP2 models. Palaeogeogr. Palaeoclimatol. Palaeoecol. 288, 93–102.
Webster, P.J., Magana, V.O., Palmer, T.N., Shukla, J., Tomas, R.A., Yanai, M., Yasunari, T., 1998. Monsoons: processes, predictability, and the prospects for prediction. J. Geophys. Res. 103 (C7), 14451–14510.
Wu, J., Shen, J., 2010. Paleoenviromental and paleoclimatic changes in Lake Xingkai inferred from stable carbon and nitrogen isotopes of bulk organic matter since 28 ka BP (in Chinese). Acta Sedimentol. Sin. 28, 365–372.
Wu, J., Shen, J., 2010. Paleoclimate evolution since 277 kaBP reflected by grain size variation of a sediment core from Lake Xingkai, northeastern Asia (in Chinese). J. Lake Sci. 22, 110–118.
Xiao, J., Xu, Q., Nakamura, T., Yang, X., Liang, W., Inouchi, Y., 2004. Holocene vegetation variation in the Daihai Lake region of north-central China a direct indication of the Asian monsoon climatic history. Quat. Sci. Rev. 23, 1669–1679.
Xiao, J., Wu, J., Si, B., Liang, W., Nakamura, T., Liu, B., Inouchi, Y., 2006. Holocene climate changes in the monsoon/arid transition reflected by carbon concentration in Daihai Lake of Inner Mongolia. The Holocene 16, 551–560.
Xiao, J.Y., Lv, H.B., Zhou, W.J., 2007. Sporopollen vegetation and environmental evolution since last glacial maximum in Dahu swamp, Jiangxi (in Chinese). Sci. China Earth Sci. 37, 789–797.
Working Group I for the Fifth Assessment Report of the Intergovernmental Panel on Climate Change, 2013. The Physical Science Basis of the 5th Assessment Report of IPCC. Cambridge University Press, New York.
Xu, Y., Xu, C.H., 2012. The projection of temperature and precipitation over China under RCP scenarios using a CMIP5 multi-model ensemble. Atmos. Oceanic Sci. Lett. 5, 527–533.
Xu, Y., Gao, X.J., Shen, Y., 2009. A daily temperature dataset over China and its application in validating a RCM simulation. Adv. Atmos. Sci. 26, 763–772.
Xu, Q., Xiao, J., Li, Y., Tian, F., Nakagawa, T., 2010. Pollen-based quantitative reconstruction of Holocene climate changes in the Daihai Lake area, Inner Mongolia, China. J. Clim. 23, 2856–2868.
Xue, J.B., Zhong, W., 2011. Holocene climate variation denoted by Barkol lake sediments in northeastern Xinjiang and its possible linkage to the high and low latitude climates. Sci. China Earth Sci. 54, 603–614.
You, Q., Kang, S., Aguilar, E., Pepin, N., Flugel, W.A., Yan, Y., Xu, Y., Zhang, Y., Huang, J., 2011. Changes in daily climate extremes in China and their connection to the large scale atmospheric circulation during 1961–2003. Clim. Dyn. 36, 2399–2417.
Zhai, P.M., Sun, A., Ren, F., Liu, X., Gao, B., Zhang, Q., 1999. Changes of climate extremes in China. Clim. Chang. 42, 203–218.
Zhai, P.M., Zhang, X.B., Wan, H., Pan, X., 2005. Trends in Total precipitation and frequency of daily precipitation extremes over China. J. Clim. 18, 1096–1108.
Zhang, C.J., Zheng, M.P., Prokopenko, A., Steffen, M., Kuang, J., Yang, Q.L., Feng, Z.D., 2007. The palaeoenvironmental variation from the high-resolution record of the holocene sediment carbonate and isotopic composition in Bosten Lake and responding to glacial activity (in Chinese). Acta Geol. Sin. 81, 1658–1671.
Zhang, C.J., Feng, Z.D., Yang, Q.L., 2010. Holocene environmental variations recorded by organic-related and carbonate-related proxies of the lacustrine sediments from Bosten lake, northwestern China. The Holocene 20, 363–373.
Zhang, W., Ming, Q., Shi, Z., Chen, G., Niu, J., Lei, G., Zhang, H., 2014. Lake sediment records on climate change and human activities in the Xingyun lake catchment, SW China. PLoS One 9, e102167.
Zhao, S.Q., 1983. A new scheme for comprehensive physical regionalization in China (in Chinese). Acta Geograph. Sin. 38, 1–10.
Zheng, W., Wu, B., He, J., Yu, Y., 2013. The East Asian Summer Monsoon at mid-Holocene: results from PMIP3 simulations. Clim. Past 9, 453–466.
Zheng, Q., Zhang, H.C., Ming, Q.Z., 2014. Vegetational and environmental changes since 15 ka BP recorded by Lake Lugu in the southwest monsoon domain (in Chinese). Quat. Sci. 34, 1314–1326.
Zhong, W., Xue, J.B., Cao, J.X., 2010. Bulk organic carbon isotopic record of lacustrine sediments in Dahu swamp, eastern Nanling mountains in south China: implication for catchment environmental and climatic changes in the last 16,000 years. J. Asian Earth Sci. 38, 162–169.
Zhou, T.J., Yu, R.C., 2006. Twentieth-century century surface air temperature over China and the globe simulated by coupled climate models. J. Clim. 19, 5843–5858.
Zhu, C., Ma, C.M., Zhang, W.Q., Zheng, C.G., Tang, L.Y., Lu, X.F., Chen, H.Z., 2006. Pollen record from Dajiuhu Basin of shennongjia and environmental changes since 15.753 ka BP (in Chinese). Quat. Sci. 26, 814–826.
Zhu, L., Wu, Y., Wang, J., Lin, X., Ju, J., Xie, M., Daut, G., 2008. Environmental changes since 8.4 ka reflected in the lacustrine core sediments from Nam Co, central Tibetan Plateau, China. The Holocene 18, 831–839.
Zhu, L., Zhen, X., Wang, J., Lü, H., Xie, M., Kitagawa, H., Possnert, G., 2009. A ~30,000-year record of environmental changes inferred from lake Chen Co, southern Tibet. J. Paleolimnol. 42, 343–358.